



NTNU – Trondheim
Norwegian University of
Science and Technology

Fuel Savings Obtained by Replacing Traditional AC-distribution Systems onboard Vessels with DC-distribution Systems

Aleksander Opdahl

Master of Science in Electric Power Engineering

Submission date: June 2013

Supervisor: Tore Marvin Undeland, ELKRAFT

Norwegian University of Science and Technology
Department of Electric Power Engineering

Abstract

Today most of the diesel-electric systems on board ships are based on an AC-distribution of the generated power. The electric power is fed directly from the synchronous generators into an AC-grid, where it is distributed to the different loads on board. This system requires a constant rotational speed to provide the grid with the rated frequency.

By introducing a DC-grid, the system no longer has to depend on constant speed. This opens the possibility to vary the speed during operations and thereby optimize the fuel-efficiency of the prime mover to the load-situation.

This thesis has investigated the fuel savings by replacing traditional AC-distribution systems on board ships with DC-distribution systems.

The DC-distribution systems that have been considered is a DC-grid supplied by three-phase, full-bridge diode rectifiers, and a DC-grid supplied by active front-end (AFE) IGBT based rectifiers.

The thesis has concluded that vessels which experience frequent low load situations will benefit from introducing an AFE based DC-distribution system on board.

The thesis has also drawn the conclusion that vessels which mostly experience high load situations, the extra cost of investing in AFE-rectifiers cannot be justified, as the fuel savings will be virtually zero at high loads. For these vessels it will be expedient to replace the AC-distribution with the less expensive diode based DC-distribution system.

Sammendrag

I dag er diesel elektriske system for det meste basert på AC distribusjon. Synkrongeneratorer leverer effekt direkte til et AC-nett som fordeler kraften til de forskjellige lastene om bord. Dette systemet krever konstant hastighet fra diesel motoren for å kunne levere riktig frekvens til samleskinnen.

Ved å introdusere DC-distribusjon om bord, vil systemet være uavhengig av hastigheten diesel motoren leverer. Dette frigjør systemet til å kunne variere hastigheten, og muliggjør optimering av diesel motorens drivstofforbruk i den aktuelle lastsituasjonen.

Denne masteroppgaven har undersøkt drivstoffbesparelsene som oppnås ved å erstatte det tradisjonelle AC-systemet med DC-system.

DC-systemene som er undersøkt er et DC-nett hvor effekten er levert av sekspuls diodelikettere, og et DC-nett hvor effekten er levert av IGBT-baserte "Active front-end" (AFE) likerettere.

Opgaven konkluderer med at fartøy som hyppig opererer under lave lastsituasjoner vil ha en fordel av å installere et DC-nett hvor effekten er levert av IGBT-baserte "Active front-end" (AFE) likerettere.

For fartøy som opererer under høyere laster, har oppgaven konkludert med at de høye kostnadene, som innstalleringen av et AFE basert DC-nett representerer, ikke kan forsvares, da drivstoffbesparelsene vil være minimale. For disse fartøyene vil det være hensiktsmessig å installere det rimeligere DC-nettet som benytter diodelikettere.

Preface

This has been a collaboration project between NTNU and Norwegian Electric Systems.

The project has been educational and has given a better understanding of the different supply systems on board ships. This is a field of research I am interested in making a career within, and the process of writing this master thesis has made me, if possible, even more motivated to enter the field of diesel electric propulsion systems.

I would like to thank my supervisor at NTNU, Tore Marvin Undeland, and my co-supervisor from Norwegian Electric Systems, Ottar Skjervheim, for help and guidance through the time I have worked with this thesis.

I also need to thank Lars Tandle Kyllingstad at SINTEF for his considerable contribution to this report.

Contents

- 1. Elements VI
 - 1.1 List of symbols for the mechanical system VI
 - 1.2 List of symbols for the electrical system VII
- 2. Introduction 1
 - 2.1 Background and motivation 1
 - 2.2 Aim and outline of the thesis 3
- 3. Fundamentals of thermodynamics 4
 - 3.1 Combustion Cycles 4
 - 3.1.1 Carnot cycle 4
 - 3.1.2 Constant volume cycle (Otto-cycle) and constant pressure cycle (Diesel-cycle) 6
 - 3.1.3 Mixed cycle (Seiliger cycle) 8
 - 3.2 Torque dependency of the heat engine's efficiency 10
- 4. Basic theory of the synchronous generator 11
 - 4.1 Excitations systems 11
 - 4.2 Load situations 13
 - 4.3 Excitation curve and saturation of the rotor 15
- 5. Power electronics 17
 - 5.1 DPF, THD and PF for non-sinusoidal waveforms 17
 - 5.2 Three-phase, full-bridge diode rectifier 19
 - 5.2.1 Area of application 19
 - 5.2.2 Ideal three-phase, full-bridge diode rectifier with no AC-side inductance 19
 - 5.2.2.1 Basic theory 19
 - 5.2.2.2 Power factor 21
 - 5.2.3 Three-phase, full-bridge diode rectifier with an AC-side inductance 22
 - 5.2.3.1 Basic theory 22
 - 5.2.3.2 Power factor 24
 - 5.2.4 Harmonics 25
 - 5.3 Active Front-end (AFE) IGBT based rectifier 26
 - 5.3.1 Introduction 26
 - 5.3.2 Working principle and mathematical description 26
 - 5.3.3 Harmonics and power factor 28
- 6. Survey of three diesel electric power supply systems 29
 - 6.1 Diesel engine and calculation model for the specific fuel oil consumption 29
 - 6.1.1 Ratings and specifications 29
 - 6.1.2 Speed limitations of the diesel engine 31

6.2 Synchronous generator	33
6.2.1 Ratings and specifications	33
6.2.2 Investigation of the excitation system	33
6.3 Diode based DC-distribution system.....	36
6.3.1 Minimum speed.....	36
6.3.1.1 Procedure for calculating of the minimum speed of the diesel generator set.....	36
6.3.2 SFOC-characteristics.....	40
6.4 AFE based DC-distribution system.....	41
6.4.1 Minimum speed.....	41
6.4.2 SFOC-characteristics.....	43
6.5 AC-based distribution system.....	44
6.5.1 Minimum speed.....	44
6.5.2 SFOC-characteristics.....	44
6.6 Comparison of the distribution systems	45
6.6.1 Diode based DC-distribution system compared to an AC-based distribution system.....	45
6.6.2 Diode based DC-distribution compared with AFE based DC-distribution	48
7. Discussion and conclusion	51
7.1 The diode based DC-distribution system compared to the traditional AC-distribution	51
7.2 The diode based DC-distribution system compared to the AFE based DC-distribution system.	51
7.3 Conclusion.....	52
9. References	53
9.1 Literature	53
9.2 Web-based literature.....	54
9.3 Literature regarding the diesel engines specifications and efficiency calculation.....	55
9.4 E-mail correspondence	55
9.5 Information obtained from standards in Simulink.....	55

1. Elements

1.1 List of symbols for the mechanical system

Symbol	Unit	Meaning
<i>b</i>	<i>m</i>	Cylinder bore
<i>c</i>	<i>kJ/kgK</i>	Specific heat capacity
<i>c_p</i>	<i>kJ/kgK</i>	Specific heat capacity for constant pressure
<i>c_v</i>	<i>kJ/kgK</i>	Specific heat capacity for constant volume
CSR	<i>kW</i>	Continuous service rating
<i>f</i>	<i>Hz</i>	Frequency
MCR	<i>kW</i>	Maximum continuous rating
<i>n</i>	<i>RPM</i>	Speed
<i>n_c</i>	.	Operating cycle, 4 for four-stroke engines
<i>P_i</i>	<i>kW</i>	Internal power in piston engines
<i>p</i>	<i>N/m² (bar)</i>	Pressure
<i>p_{me}</i>	<i>N/m² (bar)</i>	Mean effective pressure
<i>R</i>	<i>kJ/kg</i>	Gas constant
<i>T</i>	<i>K</i>	Temperature
<i>τ_i</i>	<i>Nm</i>	Torque
<i>u</i>	<i>kJ/kg</i>	Specific internal energy
<i>q</i>	<i>kJ/kg</i>	Specific quantity of heat
<i>V</i>	<i>m³</i>	Volume
<i>V_h</i>	<i>m³</i>	Swept volume
<i>v</i>	<i>m³/kg</i>	Specific volume
<i>w</i>	<i>kJ/kg</i>	Specific work
<i>ε</i>	-	Compression ratio
<i>η</i>	-	Efficiency
<i>κ</i>	-	Specific heat ratio
<i>ω</i>	<i>rad/s</i>	Angular velocity
<i>φ</i>	-	Injection ratio
<i>φ</i>	-	Pressure rise ratio

Table 1

1.2 List of symbols for the electrical system

Symbol	Unit	Meaning
A	m^2	Cross-sectional area
B	T	Magnetic flux density
E_A	V	Induced voltage (RMS, phase)
E_{LL}	V	Induced voltage (RMS, L-L)
DPF	-	Displacement power factor
f	Hz	Frequency
H	A/m	Magnetic field intensity
I_L/I_s	A	Line current
I_d	A	DC-current
L_s	H	Synchronous inductance
l_c	m	Mean path length
MMF	A	Magnetomotive force
N_c	-	Turns
n	RPM	Speed
P	W	Active power
p	-	Pole pairs
PF	-	Power factor
Q	VA_r	Reactive power
S	VA	Apparent power
THD	-	Total harmonic distortion
V	V	Line voltage (RMS, phase)
V_{LL}/V_s	V	Line voltage (RMS, L-L)
v_{comm}	V	Commutation voltage
ω	rad/s	Angular velocity
X_s	Ω	Synchronous reactance
Φ_e	Vm	Electric flux
Φ_m	Wb	Magnetic flux
μ	H/m	Permeability

Table 2

2. Introduction

2.1 Background and motivation

Since the breakthrough of diesel-electric systems in the mid-1980s many shipping companies have chosen this propulsion system for their ships. Despite the fact that the system is more expensive, and that the increased set of components between the prime mover and the propeller causes higher transmission losses, the system is often preferred over the mechanical propulsion system. The main reason for this is that after dynamic positioning entered the market there has been an increased demand of fast response and flexibility in the power distribution and motor-control. [2.1]

Dynamic positioning utilizes azimuthing thrusters and bow thrusters to maneuver the vessel. This demands that the thrusters can be placed independent of the prime mover. With a traditional mechanical power distribution system the power is distributed with a shaft directly mounted on the prime mover. This solution limits the flexibility of the placing of the thrusters, and is therefore poorly suited for dynamic positioning systems. The diesel-electric system allows the thrusters to be placed almost completely independent of the prime mover, because the power is distributed electrically through cables and not through a shaft. [2.1]

In addition to the practical benefits related to power distribution and motor-control on board, the diesel-electric system also represents environmental and safety advantages. With increased control of power flow in the system there is a possibility to optimize the loading of the prime movers, and by that reduce fuel expenses. While mechanical propulsion system can collapse due to a single failure, this is avoided with the diesel-electric system. The diesel electric system has good redundancy, where there are several power sources that can step in if the system experiences an error. The diesel-electric system also runs very quietly compared to the mechanical system because of the reduced length of shaft lines, and the prime mover's constant speed. [2.1]

Today the diesel electric system on board ships is mainly based on AC-distribution to transfer energy from the generators to the motors that drive the propulsion of the ship. The AC-power is directly fed into an AC-switchboard where the power is distributed to the different loads. Each load is equipped with a converter, which makes it possible to control of the individual motor independent of the other loads. This is a well-proven system which has many advantages concerning the fuel consumption of the main drive and control of the motor. [2.1]

Despite these positive factors, there are still some problems associated with the AC-distribution system. Energy storages in batteries or capacitors demand rectifiers. DC-loads also need rectifiers if they are to be supplied from the AC-grid. A more serious problem with the AC-distribution system is that the generator can lose synchronization and therefore cause a voltage collapse in the system. This may occur if one of the prime movers, such as a diesel engine, experiences a speed drop. The frequency and amplitude of the induced voltage are directly connected to the rotational speed of the rotor. If the rotor speed drops, the frequency and induced voltage also drops. To maintain the voltage level, the reduced rotational speed is compensated by increasing the excitation current. The drop in frequency is not possible to regulate without introducing power electronics between the generator and the grid. This means that the AC-distribution system is entirely dependent on prime movers with constant speed. [2.2]

Many of the problems concerning the power distribution on board ships can be avoided by replacing the AC-grid with a DC-grid. There are already existing electrical systems where synchronous

generators are delivering power to a DC-grid through rectifiers. The voltage can either be controlled by the excitation system or by the power electronics. [2.2]

In a DC-grid the system is no longer dependent on constant speed. This means that the frequency of the generator can be decided freely in the design phase, and be varied during operation to achieve the maximum efficiency speed of the prime-mover. Another advantage due to the frequency independency is that high speed prime-movers, like gas turbines, can be used without gears. Gears are both space and energy consuming, and therefore undesirable to have in the system. [2.2]

There is also a benefit concerning the space-saving aspect on board ships introducing the DC-grid. On board ships there is always a need to be more space- and weight-efficient in order to make space for other demands as storage room. The frequency converters that control the motors are regulated by law to be installed in the main switchboard room. The converters are very space consuming, and demands that much of the ship is designed around the electrical system. In the DC-grid there is only a need for an inverter in front of the AC-loads, which is smaller and easier to fit to the ship's design. [2.2]

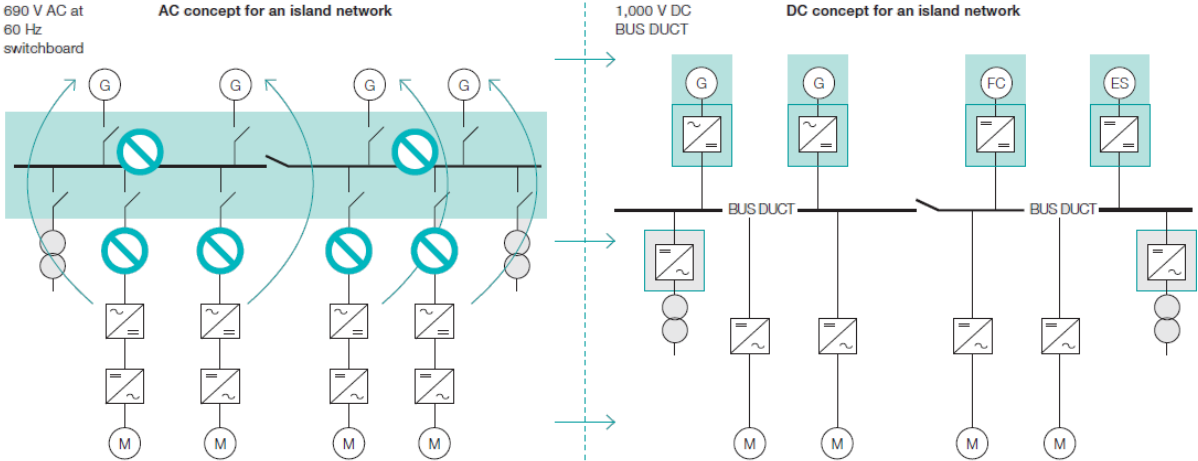


Figure 1 DC-grid compared to a traditional AC-grid [2.2]

2.2 Aim and outline of the thesis

The aim of this thesis is to decide the fuel saving by replacing traditional AC-distribution systems on board ships with DC-distribution systems.

The DC-distribution system that has been compared to the AC-distribution system is a DC-grid supplied by diode rectifiers.

The thesis also investigates the fuel savings and electrical benefits by upgrading the DC-distribution system from being supplied by diode rectifiers to being supplied by active front-end (AFE) IGBT based rectifiers.

3. Fundamentals of thermodynamics

The main purpose for varying the speed of the diesel engine is to reduce the fuel consumption. This is done by customizing the speed of the engine to the specific load that is drawn. To illustrate how the diesel engine's efficiency reacts to different speeds, the thermodynamics of the heat engine has to be presented.

3.1 Combustion Cycles

3.1.1 Carnot cycle

The first law of thermodynamics for a closed system holds that the change in specific quantity of heat dq is the sum of the change in specific internal energy du , and the change in specific work dw .

$$dq = du + dw \quad [1]$$

The change in specific energy du is a state variable and zero. This gives the expression:

$$dq = dw \quad [2]$$

dq is the differential between the supplied heat q_b , and the waste heat q_A .

The thermal efficiency can be derived from this relationship, as derived in equation 3.

$$\eta_{th} = \frac{\text{mech. work obtained } w}{\text{heat expended } q_B} = \frac{\sum q}{q_B} = \frac{q_B - q_A}{q_B} = 1 - \frac{q_A}{q_B} \quad [3]$$

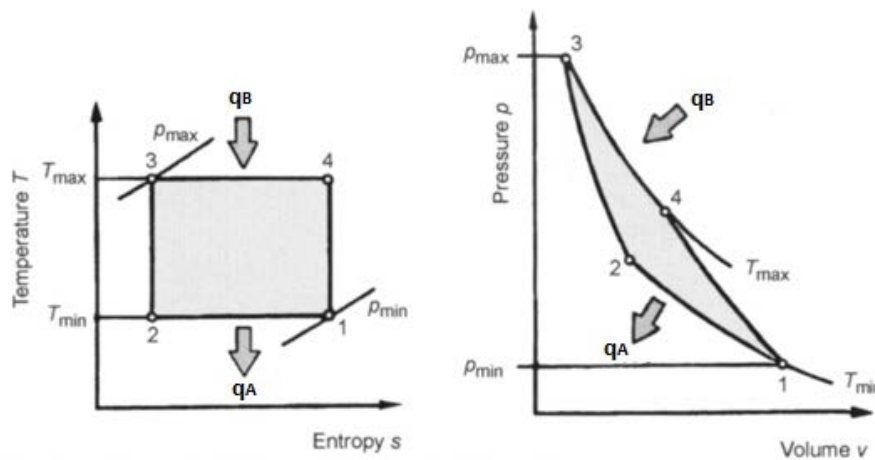


Figure 2 Combustion characteristics of the Carnot cycle [1.2]

The quantity of heat supplied to the system and the waste heat from the system can be expressed as presented in equation 4 and 5.

$$q_B = R * T_{max} * \ln \frac{v_4}{v_3} \quad [4]$$

$$q_A = R * T_{min} * \ln \frac{v_1}{v_2} \quad [5]$$

Since both the process in equation 4 and 5 are adiabatic the relationship between temperature and volume can be expressed as shown in equation 6.

$$\frac{T_{max}}{T_{min}} = \left(\frac{v_1}{v_4}\right)^{\kappa-1} = \left(\frac{v_2}{v_3}\right)^{\kappa-1} \quad [6]$$

This gives:

$$\frac{v_4}{v_3} = \frac{v_1}{v_2} \quad [7]$$

From this a temperature-dependent expression for the efficiency can be derived.

$$\eta_{th} = 1 - \frac{q_A}{q_B} = 1 - \frac{R * T_{min} * \ln \frac{v_1}{v_2}}{R * T_h * \ln \frac{v_4}{v_3}} = 1 - \frac{T_{min}}{T_{max}} \quad [8]$$

The Carnot cycle is considered the ideal process with the highest possible efficiency for a heat engine. This is because the heat is only supplied to the system at the highest temperature, while the waste heat is only given off at the lowest temperature of the process.

The efficiency of the system is independent of the heat supplied to the system. The efficiency is only dependent of the ratio between the upper temperature T_{max} , and the lower temperature T_{min} . This causes the systems efficiency to decrease as the supplied heat makes the T_{min} rise.

Another reason the Carnot cycle is an unsuited process for piston engines is the limitations in volume the piston moves in. The piston operates between top dead center (t. d. c) and bottom dead center (b. d. c). From the p-V diagram it is shown that the volume-limits also limits the mean pressure and the work that can be produced by the engine.

The volume-limits of a piston engine mean that there will be a need for very large engines to produce low outputs of work, which again causes the mechanical losses to eliminate the high thermal efficiency of the Carnot cycle. The Carnot cycle is therefore not used for piston engines. [1.1]

3.1.2 Constant volume cycle (Otto-cycle) and constant pressure cycle (Diesel-cycle)

To avoid the clear problems of the Carnot-cycle due to the piston engines limitations regarding maximum pressure, volume limitations and the increase in temperature which cause a fall in the thermal efficiency of the engine, other combustion-cycles have been developed.

The Constant-volume cycle, also known as the Otto-cycle has an efficiency that depends only on the compression ratio ε , and the isentropic exponent κ . The cylinder peak pressure increases with an increase in the input, but this is neglected. This cycle is used for spark-ignition engines, due to the spontaneous start of the combustion, which makes the pressure in the cylinder rise without a momentary expand of the volume.

The compression ratio is the ratio between the total volume over the piston when the piston is in the bottom dead center, and the volume over the piston when it is in the top dead center. The isentropic exponent is the gas's specific heat ratio, and is given by the ratio between the gas's specific heat at constant pressure C_p , and the gas's specific heat at constant volume C_v . To simplify, the specific heat ratio is set to 1.4 for all states. [1.1]

The expression for ε is shown in equation 9.

$$\varepsilon = \frac{V_h + V_c}{V_c} \quad [9]$$

The expression for V_h is expressed in equation 10.

$$V_h = \left(\frac{\pi}{4} * b^2 * s \right) \quad [10]$$

By applying equation 10 in equation 9, the expression in equation 11 is derived.

$$\varepsilon = \frac{\left(\frac{\pi}{4} * b^2 * s \right) + V_c}{V_c} \quad [11]$$

The expression for κ is:

$$\kappa = \frac{C_p}{C_v} \quad [12]$$

The efficiency of the constant-volume cycle is expressed in equation 13.

$$\eta_{thGR} = 1 - \frac{1}{\varepsilon^{\kappa-1}} \quad [13]$$

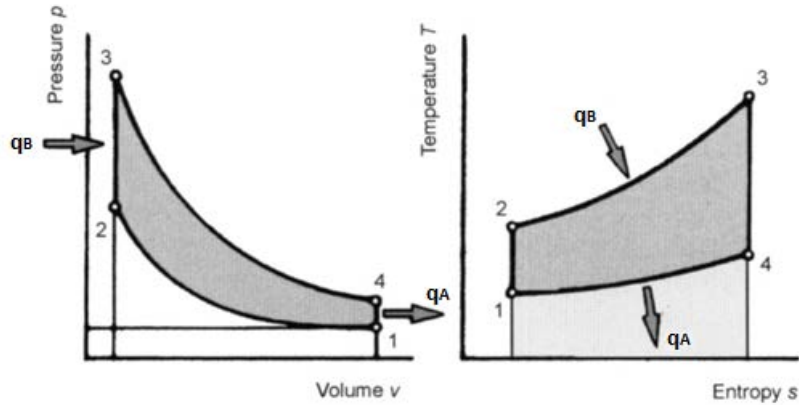


Figure 3 Combustion characteristics of the constant-volume cycle [1.2]

In the constant pressure cycle, the efficiency is not only dependent on the compression ratio and the gas's specific heat ratio, but also the injection ratio ϕ . The injection ratio is the ratio between the volume over the piston after the fuel injection and the volume over the piston before the fuel injection. [1.1]

Injection ratio:

$$\phi = \frac{V_3}{V_2} = \frac{T_3}{T_2} \quad [14]$$

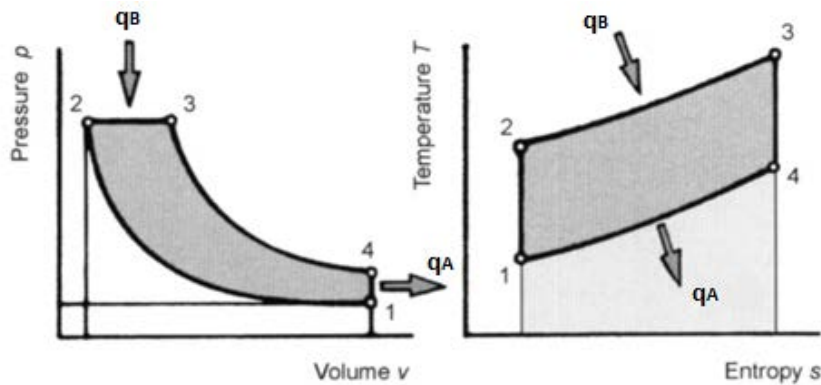


Figure 4 Combustion characteristics of the constant-pressure cycle [1.2]

In the p-V diagram it is shown that the injection ratio is dependent on the amount of heat supplied to the system, the injection ratio increases with increasing q_B . The efficiency of the constant pressure cycle is expressed in equation 15. [1.1]

$$\eta_{mtGD} = 1 - \left(\frac{1}{\kappa \epsilon^{\kappa-1}} * \frac{\phi^{\kappa} - 1}{\phi - 1} \right) \quad [15]$$

At constant compression ratio and constant heat ratio, the constant-pressure cycle's efficiency decreases as the supplied heat q_B increases. This is illustrated in figure 5.

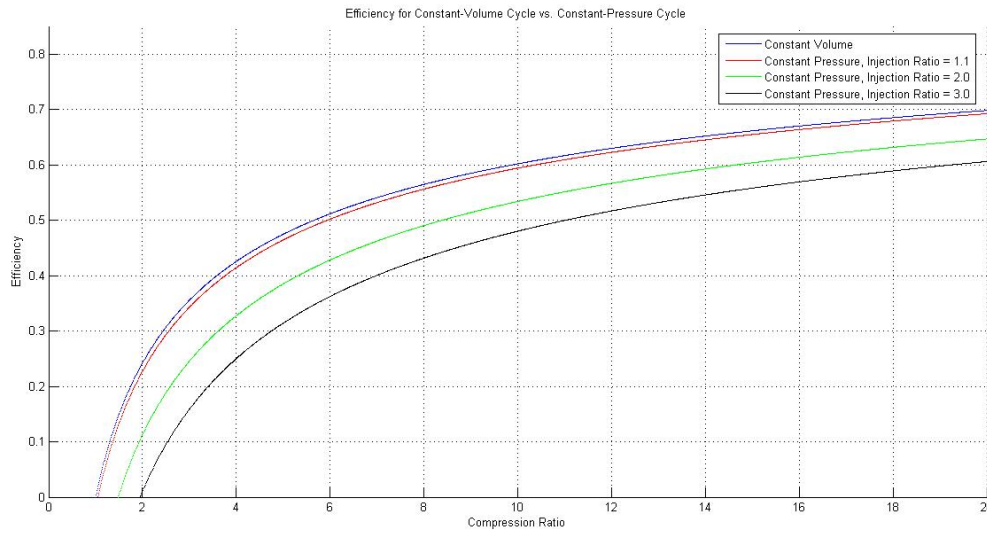


Figure 5 The constant-volume cycle compared with the constant-pressure cycle

3.1.3 Mixed cycle (Seiliger cycle)

For most diesel engines the maximum cylinder pressure is higher than the compression pressure. This opens for a combination of the constant-volume and the constant-pressure cycle, which can achieve a higher efficiency than the constant-pressure cycle.

The combustion in the mixed cycle is represented in figure 6.

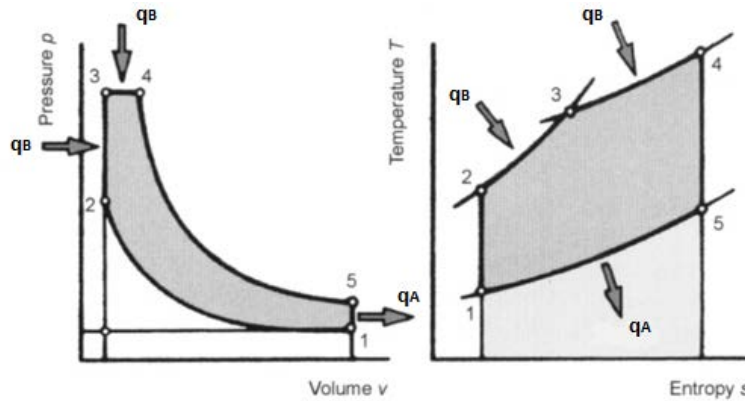


Figure 6 Combustion characteristics of the mixed cycle [1.2]

The diagram shows that the mixed cycle starts as a constant-volume cycle until the pressure has reached p_3 . The cycle converts into having a constant-pressure characteristic after p_3 is reached.

The expression for the efficiency of the mixed cycle is presented in equation 16.

$$\eta_{thS} = 1 - \left(\frac{1}{\varepsilon^{\kappa-1}} * \frac{\varphi^{\kappa} * \phi - 1}{\phi - 1 + \kappa\phi * (\varphi - 1)} \right) \quad [16]$$

Pressure rise ratio:

$$\phi = \frac{T_3}{T_2} = \frac{p_3}{p_2} \quad [17]$$

Injection ratio:

$$\varphi = \frac{T_4}{T_3} = \frac{V_4}{V_3} \quad [18]$$

The p-V diagram clearly illustrates that a decrease in the upper pressure p_3 , will cause the pressure rise ratio ϕ to decrease. A decrease in the upper pressure increases the difference between V_4 and V_3 and causes a higher injection ratio φ .

The constant-volume cycle has higher efficiency than the constant-pressure cycle. The efficiency of the mixed cycle has the constant-volume efficiency as the upper limit and the constant-pressure as lower limit.

In a mixed-cycle combustion where ϕ approaches the value one, the efficiency will be approximately equal to the efficiency of the constant-pressure cycle. [1.1]

The curves in figure 7 show how the efficiency of the mixed cycle increases with increasing pressure.

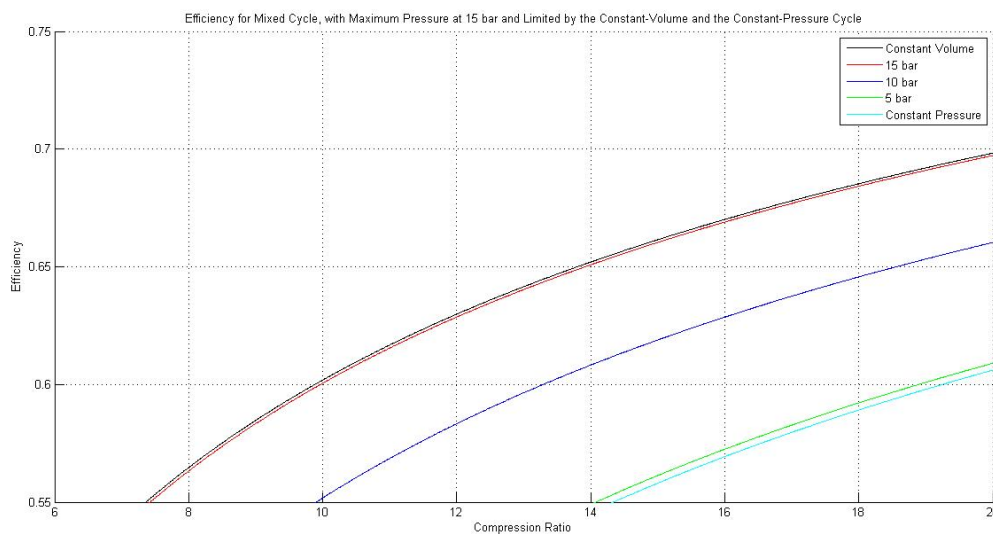


Figure 7 Efficiency of the mixed cycle at different pressures

3.2 Torque dependency of the heat engine's efficiency

The induced power per cylinder of a heat engine can be calculated as shown in equation 19.

$$P_i = p_{me} * V_h * f * \frac{1}{n_c} \quad [19]$$

The induced power can also be expressed as:

$$P_i = \tau_i * \omega \quad [20]$$

The angular speed ω is derived in equation 21.

$$\omega = 2\pi * f \quad [21]$$

By inserting equation 21 into equation 20, the expression for induced power in equation 22 is derived.

$$P_i = \tau_i * 2\pi * f \quad [22]$$

From this the pressures dependence of the torque can be derived.

$$\tau_i * 2\pi * f = p_{me} * V_h * f * \frac{1}{n_c} \quad [23]$$

This gives:

$$p_{me} = \tau_i * 2\pi * \frac{n_c}{V_h} \quad [24]$$

2π , n_c and V_h are constants, which give:

$$2\pi * \frac{n_c}{V_h} = k \quad [25]$$

This means that the pressure is only dependent of the torque, and increases linearly with an increasing torque.

$$p_{me} = k * \tau_i \quad [26]$$

As presented in the previous chapter, the efficiency of the mixed cycle increases with an increasing pressure. From this it is clear that the engine has to operate at highest possibly torque to achieve its highest efficiency. The expression in equation 20 shows that the maximum torque is achieved at lowest possible speed. [1.1]

4. Basic theory of the synchronous generator

The synchronous generator is the most common generator in diesel electric systems. In this thesis the principle behind the generator will not be presented. The focus will be on the excitation system and saturation of the rotor as this is most relevant to the topic of the thesis.

4.1 Excitations systems

There are two methods to excite the rotor windings, excitation with brushes and slip-rings, and excitation without brushes, called brushless excitation. The excitation system supplies the rotor windings with a DC-current, which again provides the magnetic field that induces the voltage in the stator windings. Assuming that there is no magnetic saturation in the rotor, the induced voltage E is linearly dependent on the excitation current that is fed in to the rotor. The excitation system should under all load conditions be able to deliver the necessary excitation current to provide the right output AC-voltage, and quickly regulate for speed variations and load changes.

The first excitation systems consisted of a DC-generator directly coupled to the synchronous machines shaft. Due to the rapid development of rectifiers in the 1950s these systems were left for new systems with AC-generators.

To achieve a fast regulation of the induced voltage in the stator, there are two excitation-generators, a main-exciter and a pilot-exciter being used. Both are coupled to the synchronous generators shaft, similar to the old system with a DC-generator. The main-exciter generates the excitation current, while the pilot-exciter produces the control signal which regulates the excitation current. There are also systems that use static exciters. These exciters do not consist of any rotating parts.

Excitation systems can use brushes and slip rings to deliver a DC-current to the rotor. This is a very simple system, but requires much maintenance. The brushes get worn-out and must frequently be cleaned, repaired or replaced. To avoid this constant need for maintenance, a brushless excitation system has been developed. This system is more expensive, but it is almost maintenance free compared to the generators with brushes and slip rings. [1.3]

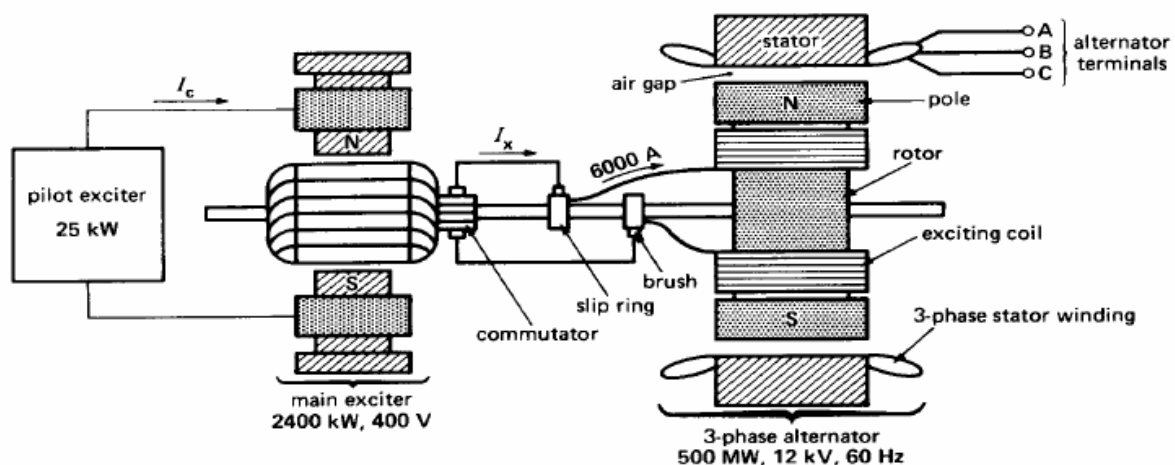


Figure 8 Cross section of a synchronous generator with slip rings [2.3]

In the brushless system the main-excitation generator has poles that stand still, while the armature is rotating. The armature is mounted on the shaft of the main-generator, together with a thyristor-rectifier. To control the excitation current, there is a pulse transformer mounted on the generator. The pulse transformer has one stationary winding on the armature, and one rotating winding on the shaft. The pulse transformer gives a signal to the thyristor-rectifier, which trigger the ignition to the thyristors. This provides a controllable excitation current, which means that the induced voltage in the armature of the main-generator also is controllable. Because of the pulse transformer there is no need for brushes or slip-rings to transfer the ignition-pulse to the generator's rotor. This machine is, in addition to being called a brushless synchronous machine, also called a generator with rotating rectifier. [1.3]

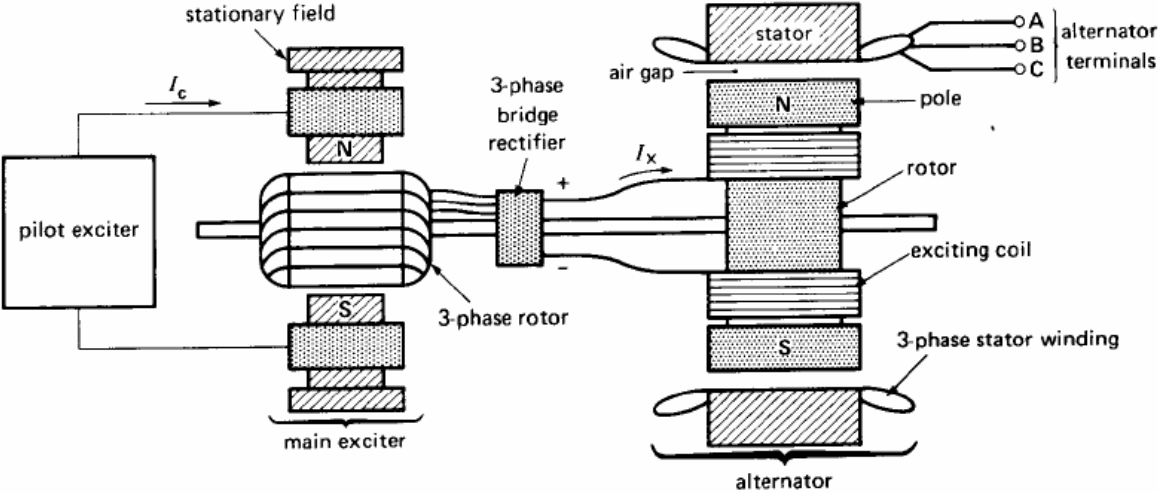


Figure 9 Cross section of a brushless synchronous generator [2.3]

4.2 Load situations

In no-load operation there is no angle between the induced voltage E and the terminal voltage V . When the synchronous machine is loaded, the current in the armature will create losses in the stator windings. Due to the windings' relative high reactance compared to the windings' resistance, the loss is assumed to be purely reactive. This loss causes an angle between the induced voltage E and the terminal voltage V .

When the load is purely resistive the generator needs to deliver a current with a power factor equal to one. When the rotor turns to induce the voltage in the armature, the poles shift an angle β from its position in no-load operation. The armature MMF \vec{F}_a is ahead of the rotors MMF \vec{F}_{mL} . This causes the armature MMF \vec{F}_a to have a negative sign in the expression in equation 27.

$$\vec{F}_r = \vec{F}_{m0} = \vec{F}_{mL} + \vec{F}_a \quad [27]$$

To maintain the voltage at the terminals at the same level as in no-load operation, the resulting flux Φ_r needs to be the same as the magnetic flux Φ_m in no-load operation. To achieve this, the machine needs to compensate the negative \vec{F}_a with a larger \vec{F}_{mL} . This is done by increasing the excitation current. [1.3]

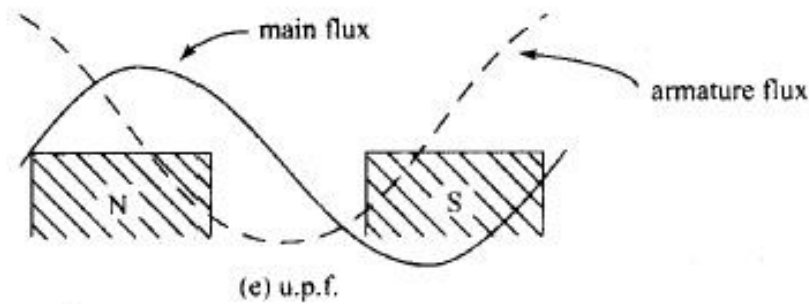


Figure 10 Main flux and armature flux at resistive load [2.4]

When the load is purely inductive the power factor is zero. In other terms the armature current is lagging 90 degrees to the voltage. In this case there is no angle between the induced voltage E and the voltage at the terminal U . Due to the 90 degree lag, the armature MMF is working directly against the rotors MMF. To maintain the same voltage at the terminals as in the no-load operation the rotors MMF \vec{F}_{mL} has to be increased. This is achieved in the same way as in the situation with the purely resistive load; the excitation current in the rotor is increased. [1.3]

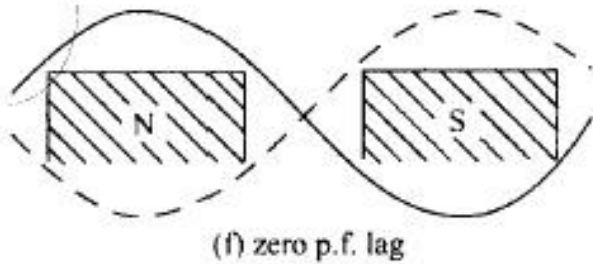


Figure 11 Main flux and armature flux at inductive load [2.4]

In situations where the load is purely capacitive the armatures MMF will work in the same direction as the rotors MMF. This means that in order to achieve the same voltage at the terminals as in the no-load operation, the rotor MMF \vec{F}_{mL} has to be reduced by decreasing the excitation current. [1.3]

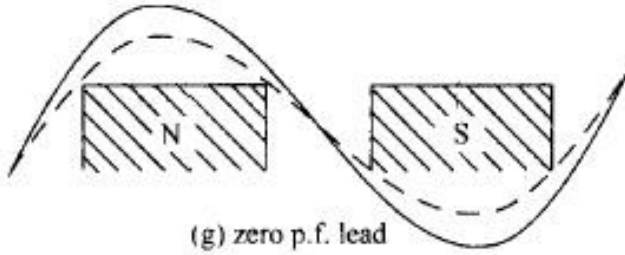


Figure 12 Main flux and armature flux at capacitive load [2.4]

4.3 Excitation curve and saturation of the rotor

The induced voltage in the stator depends on the strength of the flux and the rotational speed of the rotor. The flux increases linearly with the excitation current until the iron in the rotor is saturated. When the iron in the rotor is saturated the flux strength will not increase with the excitation current, but flatten out.

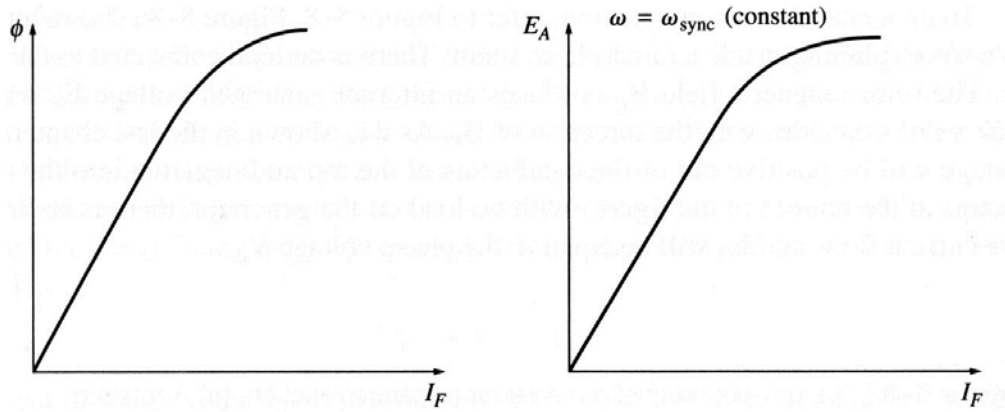


Figure 13 Saturation curve for the rotor [2.5]

The magnitude of the induced voltage in each of the stator phases is expressed in equation 28.

$$E_A = \sqrt{2}\pi N_C \phi f \quad [28]$$

The frequency is calculated as shown in equation 29.

$$f = \frac{n * p}{60} \quad [29]$$

As seen from equation 28 and 29, a drop in the speed n , can be compensated by increasing the flux strength until the iron in the rotor is saturated.

The relationship between the flux and the excitation current is presented in equation 30.

$$\phi = \frac{\mu * N_C * I_F * A}{l_c} \quad [30]$$

Equation 29 and equation 30 are inserted in equation 28. This gives the expression:

$$E_A = \sqrt{2}\pi N_C * \frac{\mu * N_C * I_F * A}{l_c} * \frac{n * p}{60} \quad [31]$$

$\sqrt{2}\pi$, N_C , A , l_c and $\frac{p}{60}$ are constants, and expressed by the constant C .

$$C = \frac{\sqrt{2}\pi * N_C^2 * A * p}{l_c * 60} \quad [32]$$

The permeability μ is given by the ratio between the magnetic flux density B and the magnetizing intensity H .

$$\mu = \frac{B}{H} \quad [33]$$

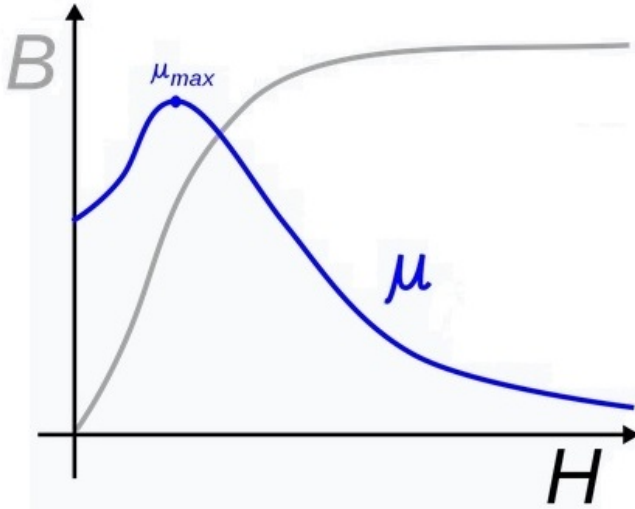


Figure 14 B-H curve [2.6]

As seen in figure 14, the magnetic flux density flattens out as the iron is saturated, and as a direct consequence the permeability decreases.

The constant C and the permeability are combined to the factor K .

$$K = \mu * C \quad [34]$$

This factor will consequently also decrease as the iron in the rotor is saturated.

By inserting equation 34 into equation 31, the induced voltage per phase can be expressed as shown in equation 35.

$$E_A = K * I_F * n \quad [35]$$

The factor K can be expanded to include $\sqrt{3}$. The expression will then give the induced line to line voltage E_{LL} . [1.4]

5. Power electronics

The two rectifiers that are applied in this thesis is the six-pulse diode rectifier and the active front-end (IGBT) based rectifier. The theory regarding their working principle, generated harmonics and efficiency is presented in the following chapters.

5.1 DPF, THD and PF for non-sinusoidal waveforms

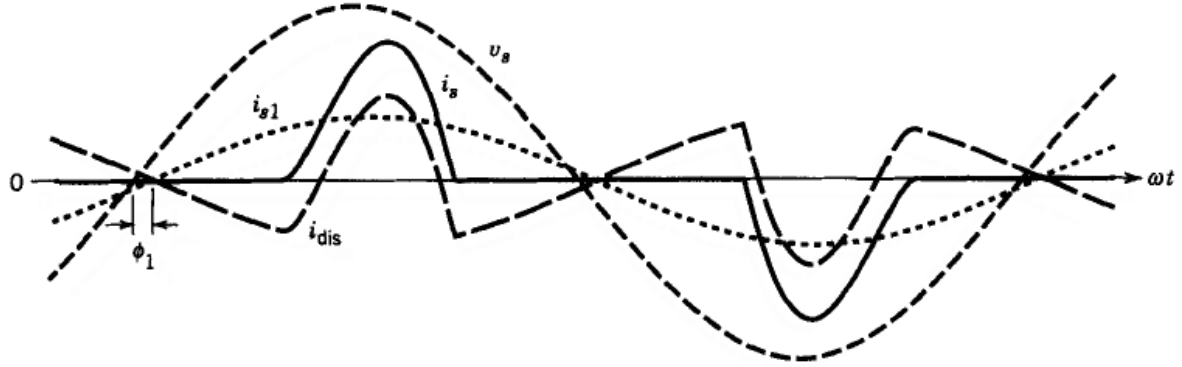


Figure 15 Line-current distortion [1.5]

The displacement power factor (DPF) is the cosine of the angle between the sinusoidal input voltage v_s and the fundamental frequency component of the line current I_{s1} . I_s is the RMS value of the line current.

$$DPF = \cos \phi_1 \quad [36]$$

The distortion component of the line current is expressed in equation 37.

$$I_{dis} = \sqrt{I_s^2 - I_{s1}^2} \quad [37]$$

The total harmonic distortion in the current (THD_i) is the ratio between the distortion component and the fundamental frequency component of the line current. This is derived in equation 38.

$$THD_i = \frac{I_{dis}}{I_{s1}} = \frac{\sqrt{I_s^2 - I_{s1}^2}}{I_{s1}} \quad [38]$$

The power factor (PF) is calculated as for a sinusoidal state.

$$PF = \frac{P}{S} \quad [39]$$

The active power is given by the expression:

$$P = \sqrt{3} * V_s * I_{s1} * \cos \varphi_1 \quad [40]$$

The apparent power is expressed by in equation 41:

$$S = \sqrt{3} * V_s * I_s \quad [41]$$

The power factor is then derived by inserting the expressions in equation 40 and 41 into the expression in equation 39.

$$PF = \frac{\sqrt{3} * V_s * I_{s1} * \cos \varphi_1}{\sqrt{3} * V_s * I_s} = \frac{I_{s1}}{I_s} * DPF \quad [42]$$

Due to the relationship between the THD_i , and I_{s1} and I_s presented in equation 38, the ratio between I_{s1} and I_s can be expressed by the THD_i .

$$\frac{I_{s1}}{I_s} = \frac{1}{\sqrt{1 + THD_i^2}} \quad [43]$$

This gives the expression:

$$PF = \frac{1}{\sqrt{1 + THD_i^2}} * DPF \quad [44]$$

[1.5]

5.2 Three-phase, full-bridge diode rectifier

5.2.1 Area of application

In systems where a stable three-phase voltage is available, the three-phase, full bridge diode rectifier is most common. These rectifiers do not provide any control of the output DC-voltage, but have relatively low cost and are robust compared to other AC-DC converters which provide controlled DC-output. [1.5]

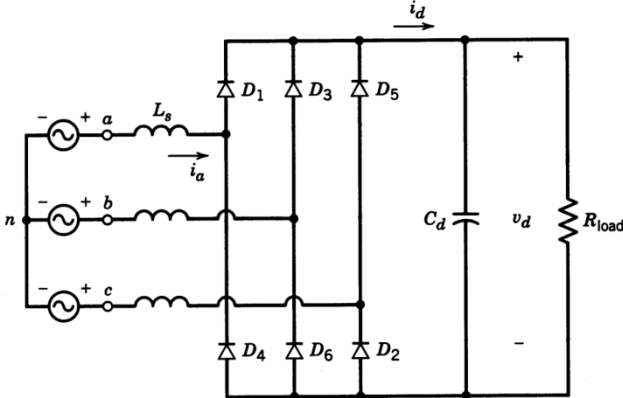


Figure 16 Three-phase, full-bridge diode rectifier [1.5]

5.2.2 Ideal three-phase, full-bridge diode rectifier with no AC-side inductance

5.2.2.1 Basic theory

The three-phase, full bridge diode rectifier consists of six diodes in a three-phase circuit. To simplify the working principle of the rectifier, the circuit is assumed to be ideal. The inductance L_s on the AC-side is neglected to avoid delayed current commutation. The load on the DC-side is replaced by a constant DC-current. Replacing the constant DC-current with a resistive load will not have a severe effect on the result of the calculations. [1.5]

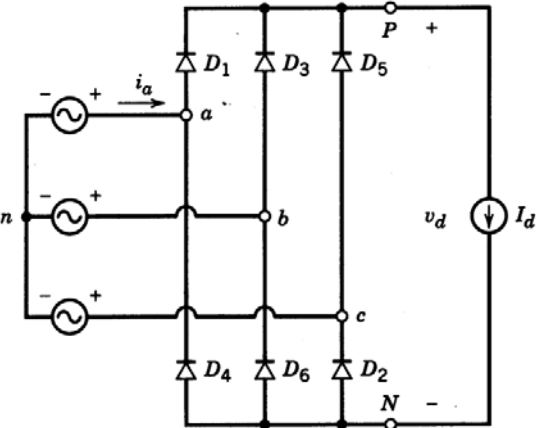


Figure 17 Ideal three-phase, full-bridge diode rectifier with constant DC-current [1.5]

Which diode conducts is determined by where the highest and lowest potential is at any given time. The diodes on the upper-side of the circuit are dependent on having the highest potential at their anode to conduct. The diode with the highest potential at its anode is conducting, while the two other diodes become reversed biased. The diodes on the low-side of the circuit will conduct if they have the lowest potential of the three diodes on their cathode. The two other diodes become reversed biased, and block. [1.5]

Pulse number	Conducting diode	Current transition
1	D6	D5 to D1
2	D1	D6 to D2
3	D2	D1 to D3
4	D3	D2 to D4
5	D4	D3 to D5
6	D5	D4 to D6

Table 3 Sequence of the diodes conducting and blocking [1.6]

This sequence of conducting and blocking, gives an output DC-voltage v_d , with six pulses, each with a width of $\frac{\pi}{3}$, per period. The DC-voltage v_d is defined as the difference between the voltage v_{Pn} and the voltage v_{Nn} . [1.5]

$$v_d = v_{Pn} - v_{Nn} \quad [45]$$

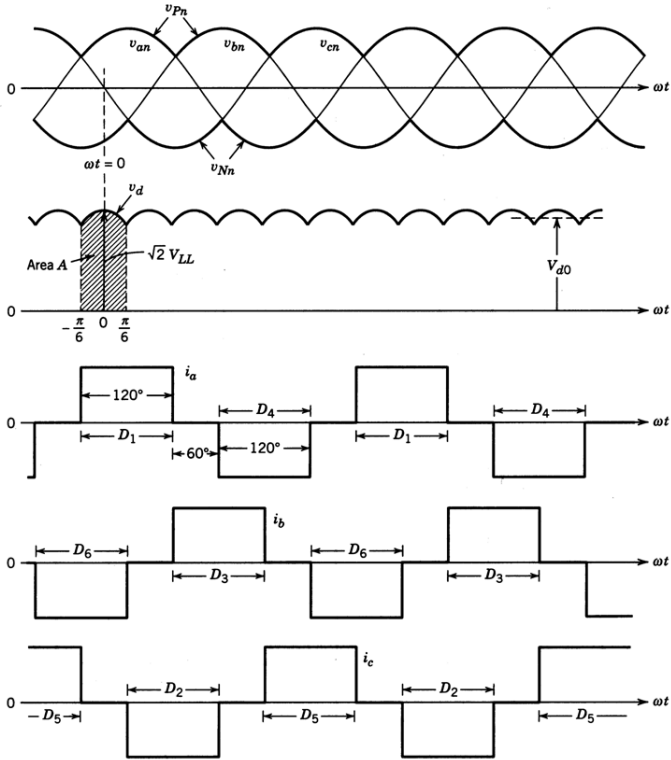


Figure 18 Waveforms of the rectifier [1.5]

From the second waveform it can be seen that the peak value of v_d is equal to the peak value of the line to line voltage v_{ab} . This means that the average value of the voltage on the DC-side V_{d0} can be calculated by integrating v_{ab} from $-\frac{\pi}{6}$, to $\frac{\pi}{6}$, and then divide by the length of the interval. [1.5]

$$V_{d0} = \frac{1}{\pi} \int_{-\frac{\pi}{6}}^{\frac{\pi}{6}} \sqrt{2} * V_s * \cos \omega t d(\omega t) = \frac{3}{\pi} \sqrt{2} V_s \quad [46]$$

5.2.2.2 Power factor

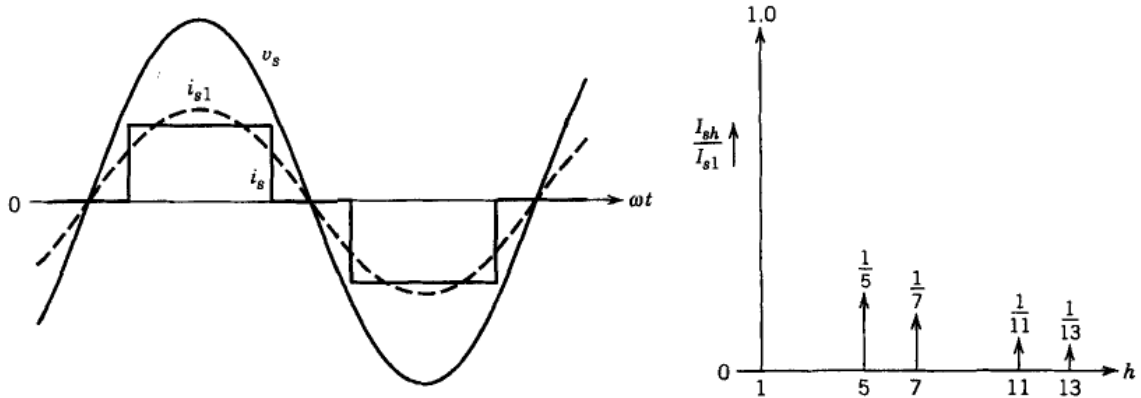


Figure 19 Line current for an ideal three-phase, full-bridge diode rectifier with no AC-side inductance [1.5]

In an ideal circuit with no AC-side inductance, I_{s1} and I_s can be expressed as presented below:

$$I_{s1} = \frac{1}{\pi} * \sqrt{6} * I_d \quad [47]$$

$$I_s = \sqrt{\frac{2}{3}} * I_d \quad [48]$$

The displacement power factor (DPF) is 1 in the ideal state, as I_{s1} is in phase with V_s . [1.5]

$$PF = \frac{I_{s1}}{I_s} * DPF = \frac{\frac{1}{\pi} * \sqrt{6} * I_d}{\sqrt{\frac{2}{3}} * I_d} * 1 = \frac{3}{\pi} = 0.955 \quad [49]$$

5.2.3 Three-phase, full-bridge diode rectifier with an AC-side inductance

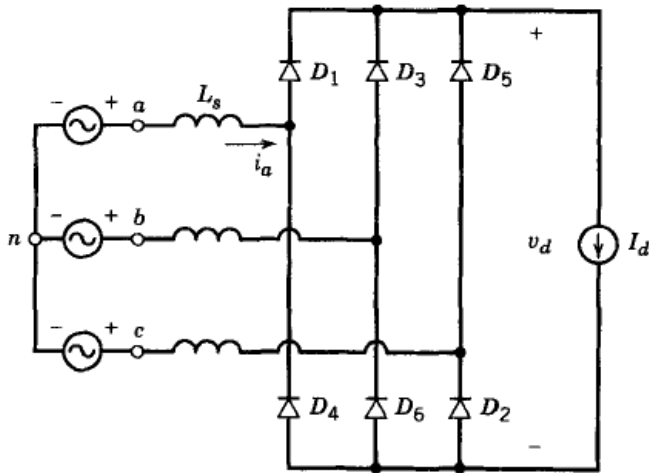


Figure 20 Three-phase, full-bridge diode rectifier with an AC-side inductance [1.5]

5.2.3.1 Basic theory

In a circuit with an AC-side inductance the phase current I_{phase} is not able to instantaneously switch from a positive direction (I_d) to a negative direction ($-I_d$). The current commutation will therefore be delayed, and there will be a voltage drop in the rectifier. [1.5]

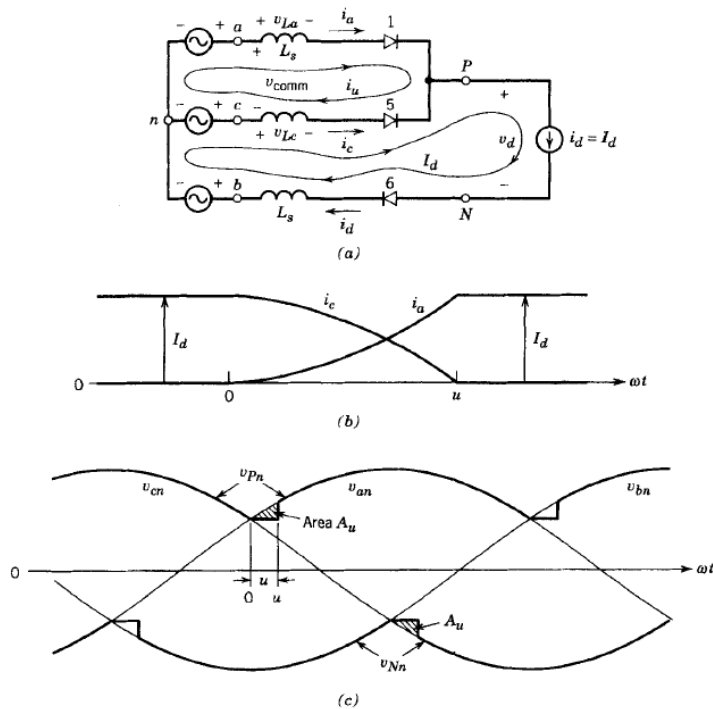


Figure 21 Commutation process from diode 5 to diode 1 [1.5]

The commutation voltage is the difference between the two phase voltages v_{an} and v_{cn} .

$$v_{comm} = v_{an} - v_{cn} \quad [50]$$

The phase currents are expressed in equation 51 and 52.

$$i_a = i_u \quad [51]$$

$$i_c = I_d - i_u \quad [52]$$

The commutation current builds up from zero at the start of the commutation interval to I_d when the commutation is completed.

The integral of the voltage drop during the commutation is expressed in equation 53.

$$A_u = \omega L_s \int_0^{I_d} di_u = \omega L_s I_d \quad [53]$$

This area is lost at every interval, which consist of 60° ($\frac{\pi}{3}$ rad.). The average voltage drop for each interval is therefore:

$$\Delta V_d = \frac{\omega L_s I_d}{\frac{\pi}{3}} = \frac{3}{\pi} \omega L_s I_d \quad [54]$$

The average output DC-voltage will be the DC-voltage with instantaneous commutation minus the average voltage drop due to the delayed commutation.

$$V_d = V_{d0} - \Delta V_d = \frac{3}{\pi} \sqrt{2} V_s - \frac{3}{\pi} \omega L_s I_d \quad [55]$$

5.2.3.2 Power factor

To simplify the calculations it is assumed that the output DC-voltage of the rectifier is constant.

With a delayed current commutation the displacement angle is not zero, as I_{s1} is not in phase with V_s .

The RMS values of I_{s1} and I_s cannot be expressed as shown in expression 47 and 48 when an inductance is introduced on the AC-side. The phase current is depending on the commutation current, as expressed in equation 51 and 52. This will severely complicate the calculations. [1.5]

Due to the complicated calculation, this thesis has applied a graphical solution to find the power factor for each load.

The ratio between V_d and V_{d0} is calculated. It is assumed that I_d is constant. From this value the ratio between I_d and the short circuit current I_{sc} is obtained from the graph in figure 22.

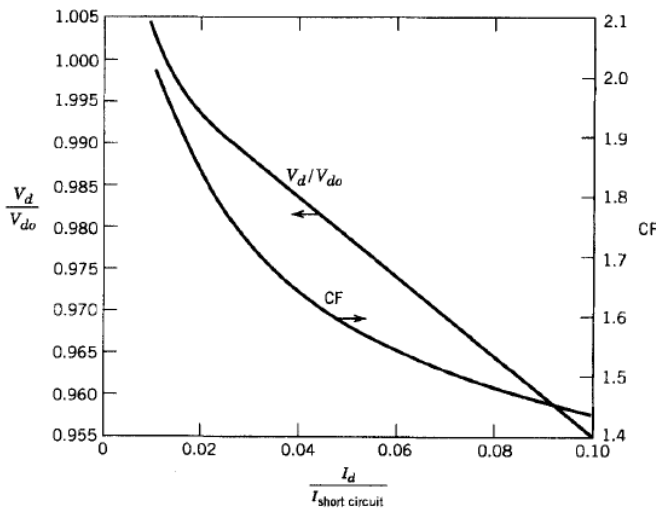


Figure 22 [1.5]

The ratio between I_d and I_{sc} is then used to find the power factor from the graph in figure 23.

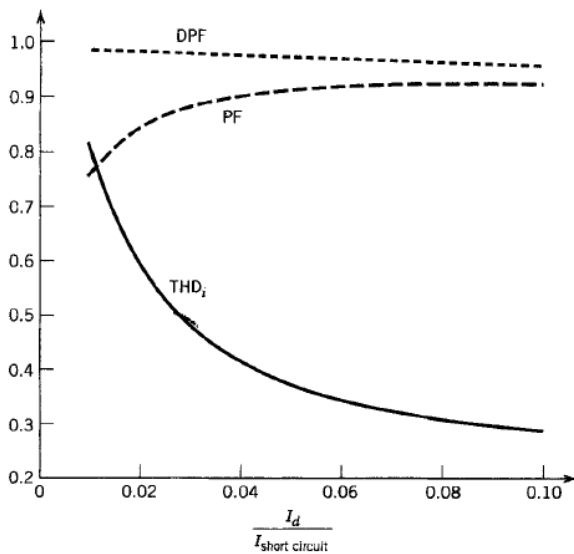


Figure 23 [1.5]

5.2.4 Harmonics

The diode rectifier draws a current with a high amount of harmonics. This causes the current to be far from sinusoidal. The power factor also gets affected negatively by the large number of harmonics.

The low power factor can cause severe problems for the supply system, such as large load currents. The high load current increases the losses in the armature windings. The system may also not be suited for the high load currents, and it will cause a breakdown in the system. [1.5]

On board ships the maximum power that can be drawn is limited by the size of the diesel engine. Breakdown due to high currents caused by poor power factor is therefore not a relevant issue.

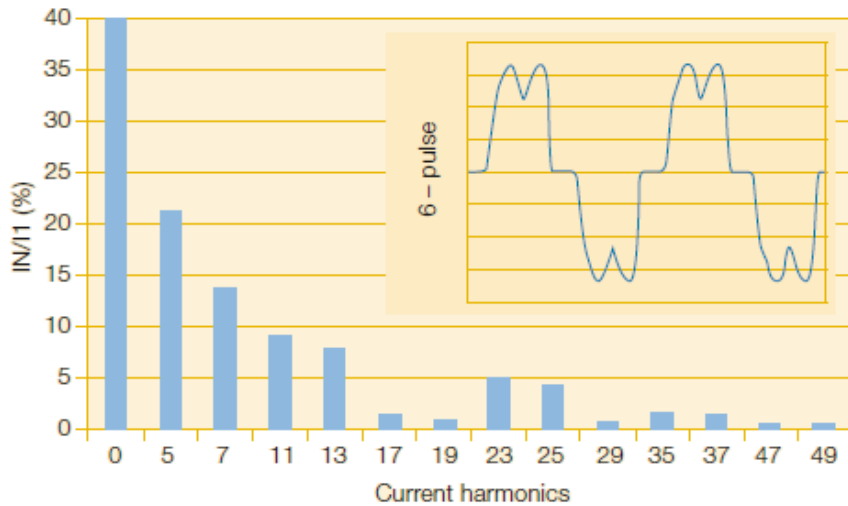


Figure 24 [2.7]

5.3 Active Front-end (AFE) IGBT based rectifier

5.3.1 Introduction

The introduction of fully controlled power switches like IGBTs or power MOSFETs makes it possible to use pulse width modulation to control the output DC-voltage. The IGBT is mainly used because of its excellent combination of high switching frequency and low on-state losses. [1.5]

5.3.2 Working principle and mathematical description

The voltage-type (boost), PWM rectifier is supplied by three input inductors on the ac-side. The inductors are needed to boost the output DC-voltage above the input line voltage. This is one of the biggest advantages with the AFE; the DC-side voltage can be varied from the peak value of the input voltage, to a theoretical unlimited output voltage. For practical purposes the maximum output voltage is limited to a value around ten times the peak value of the input voltage.

The biggest disadvantage with the AFE is that the high switching frequency represents a relative high power loss. The expression for the switching power loss P_s is given in equation 56. [1.5] [1.7]

$$P_s = \frac{1}{2} V_d I_0 f_s (t_{c(on)} + t_{c(off)}) \quad [56]$$

As seen in this expression the power loss due to switching increases with the switching frequency f_s .

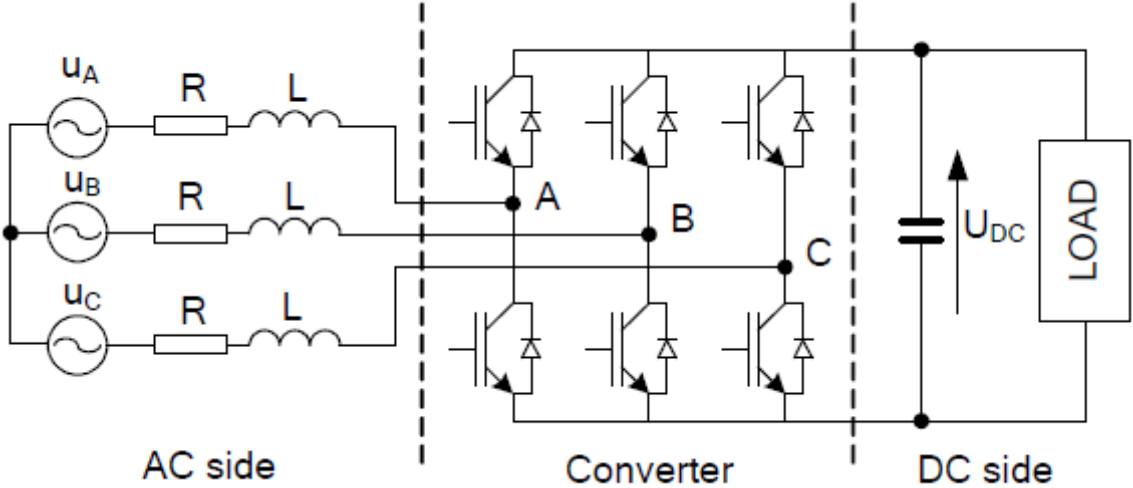


Figure 25 Three-phase, active front-end (AFE) IGBT based rectifier [2.8]

The equivalent equation of the AFE rectifier is derived by replacing each IGBT-switch with a dependent voltage and current source. The new equivalent circuit is presented in figure 26. The duty cycle for the upper IGBT-switches is defined as M_a , M_b and M_c , while the load is replaced by a dependent current source. [1.7]

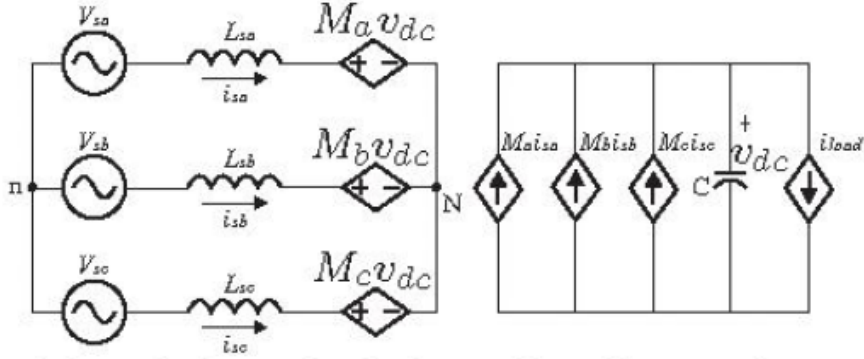


Figure 26 Equivalent circuit in an abc reference frame [1.7]

From this equivalent circuit the following expressions can be derived:

$$V_{sa} = L_{sa} \frac{di_{sa}}{dt} + M_a v_{dc} - v_{nN} \quad [57]$$

$$V_{sb} = L_{sb} \frac{di_{sb}}{dt} + M_b v_{dc} - v_{nN} \quad [58]$$

$$V_{sc} = L_{sc} \frac{di_{sc}}{dt} + M_c v_{dc} - v_{nN} \quad [59]$$

v_{nN} can be expressed as:

$$v_{nN} = \frac{1}{3} (M_a + M_b + M_c) v_{dc} \quad [60]$$

This gives the equation:

$$M_a i_{sa} + M_b i_{sb} + M_c i_{sc} = C \frac{dv_{dc}}{dt} + i_{load} \quad [61]$$

[1.7]

5.3.3 Harmonics and power factor

A big advantage with the AFE is the low ripple on the output DC-voltage due to the capacitor placed in parallel with the load. The on and off time of the switches can control both the amplitude and phase shift of the converter voltage v_c . With control of the converter voltage, the amplitude and phase of the line current can be regulated, which gives the opportunity to reduce the amplitude of the harmonics generated, making the current drawn by the rectifier approximately sinusoidal. [1.5]

The low amount of harmonics and the approximately zero displacement angle will, by applying the expression in equation 44, cause the active front-end rectifier to have a high power factor. The AFE's power factor is considered one in this thesis.

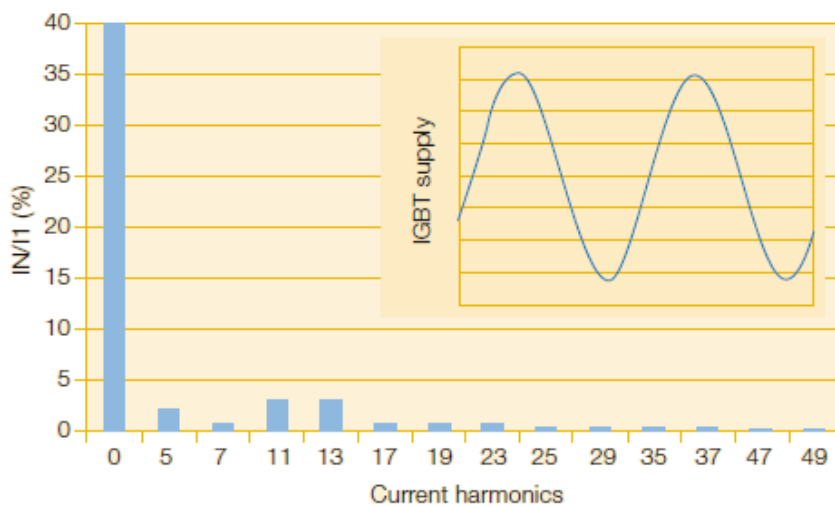


Figure 27 [2.7]

6. Survey of three diesel electric power supply systems

To obtain the fuel savings by introducing DC-grid on board vessels, three different supply systems are investigated. The supply systems that has been investigated is a DC-grid supplied by six-pulse diode rectifiers, a DC-grid supplied by active front-end (AFE) rectifiers, and an AC-grid with fixed speed at 900 RPM. All three supply systems consist of three identical diesel generator sets. In this survey the load is always equally divided between the running generators.

In the DC-grid supplied by diode rectifiers the power factor's effect on the total load and the power loss in the rectifiers is neglected.

In the DC-grid supplied by AFE rectifiers, the rectifiers switching power loss and the power loss during the on-state is neglected.

These assumptions are made to simplify the calculations of the SFOC.

The simplification of the calculations will cause the fuel savings to be somewhat higher than the actual fuel savings the introduction of DC-grid represents.

6.1 Diesel engine and calculation model for the specific fuel oil consumption

In this thesis the prime mover that will be considered is the Wärtsilä 9L20. This is a 4-stroke, non-reversible, turbocharged and intercooled diesel engine with direct fuel injection. [3.1]

6.1.1 Ratings and specifications

The ratings and specifications of the engine are presented in the table below.

Cylinder bore	200 mm
Stroke	280 mm
Cylinders	9, in-line
Speed	900 RPM
MCR	1665 kW
CSR	1415 kW
SFOC_{CSR}	190 g/kWh

Table 4 [3.1]

To determine the fuel savings the fisheries and aquaculture branch of SINTEF has provided a calculation model for the specific fuel oil consumption of different diesel engines. The model is a regression of the fuel consumption characteristics at different speed and load for several diesel engines to provide a general fuel consumption curve. The expression is presented in equation 62.

$$SFOC \approx A + B * CB + C * RPM + D * kWcylModel + E * LoadModel + F * LoadModel^2 + G * LoadModel^3 + H * LoadModel^4 + I * LoadModel^5 + J * LoadModel^6 + K * MCR + L * MCRcyl + M * p_{me} \quad [62] \quad [3.2]$$

The parameters of the model are presented in table 5.

Parameter	Description	Unit	Remarks
<i>CB</i>	Cylinder Bore	mm	Constant
<i>CS</i>	Cylinder Stroke	mm	Constant
<i>RPM</i>	Engine Turning Speed	min ⁻¹	Variable
<i>Load</i>	Engine Load	kW	Variable
<i>kWcyl</i>	Cylinder Output	kW	Variable
<i>MCR</i>	Engine Maximum Continuous Rating	kW	Constant
<i>MCRcyl</i>	Engine Maximum Continuous Rating per Cylinder	kW	Constant
<i>LoadModel</i>	<i>Load/MCR</i>	-	Variable
<i>kWcylModel</i>	<i>kWcyl/MCRcyl</i>	-	Variable
<i>p_{me}</i>	Engine Mean Effective Pressure	bar	Variable

Table 5 [3.2]

$$p_{me} = \frac{kWcyl * n_c * 1.2 * 10^9}{CB^2 * CS * RPM * \pi} [63] [3.2]$$

The constants in the expression are decided from the diesel engines cylinder size and power per cylinder. This thesis considers medium speed engines, which in the model is divided into four groups.

Description	Size	Power per cylinder
Small Bore (SB)	160 mm – 225 mm	10 kW – 250 kW
Small-Medium Bore (SMB)	226 mm – 300 mm	225 kW – 550 kW
Medium Bore (MB)	301 – 400 mm	400 kW – 750 kW
Large Bore (LB)	> 400 mm	> 750 kW

Table 6 [3.2]

The bore and power per cylinder of the W 9L20 is respectively 200 mm and 185 kW. The engine is therefore defined by the SFOC-model as a "small bore" engine. The SFOC-model's constants for an engine with small bore are given in table 7.

Constant	Value
A	203.541500
B	0.874700
C	0.104600
D	- 0.032810
E	- 1093.000000
F	2111.000000
G	- 2076.000000
H	847.200000
I	- 63.840000
J	0.000000
K	- 0.004478
L	- 0.484600
M	3.330000

Table 7 [3.2]

To adjust the model to suit the engine that is applied in the system, the interception value A is calculated by inserting the given values of the engine when it runs at CSR.

$$A = SFOC_{CSR} - (B * CB + C * RPM_{CSR} + D * kWcylModel + E * LoadModel + F * LoadModel^2 + G * LoadModel^3 + H * LoadModel^4 + I * LoadModel^5 + J * LoadModel^6 + K * MCR + L * MCRcyl + M * p_{me}) [64] [3.2]$$

6.1.2 Speed limitations of the diesel engine

The propulsion system is running with a fixed pitch propeller (FPP). The operating field for this configuration is presented in figure 28. [3.1]

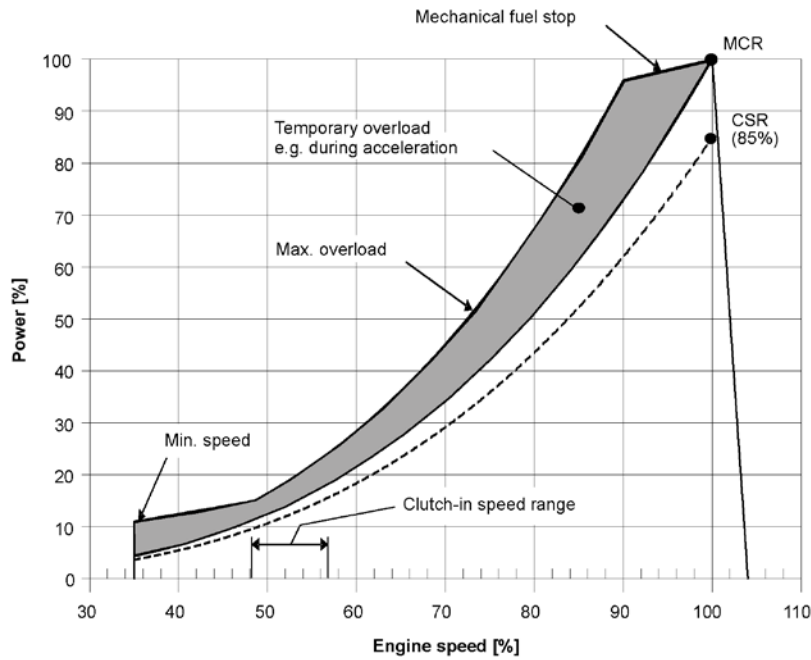


Figure 28 [3.1]

The maximum output power can be expressed approximately as a cubic function of the speed [4.1]

$$P = k_{mec} * n^3 [65]$$

The constant k_{mec} is found by inserting the values for the engine at MCR:

$$k_{mec} = \frac{MCR}{n_{MCR}^3} [66]$$

When the values obtained by the expression in equation 65 deviates from the values found in the graph in figure 28, the value from the expression is used.

The minimum speed is as shown in figure 28, 35% of the maximum speed.

$$n_{mec_{min}} = 35\% * \frac{900 \text{ RPM}}{100\%} = 315 \text{ RPM} [67]$$

In this thesis the lowest load situation that will be considered is at 75 kW. The minimum speed for this load situation is calculated in equation 67 by solving the expression in equation 65 with respect to n .

$$n_{mec_{75 \text{ kW}}} = \sqrt[3]{\frac{75}{k_{mec}}} = 320.23 \text{ RPM} [68]$$

$$n_{mec_{min}} < n_{mec_{75 \text{ kW}}} [69]$$

The calculation in equation 68 shows that speed of the diesel engine will not go below its minimum level in this thesis.

The SFOC- model in combination with the operation field limitations is used to create a graph that illustrates the engines minimum SFOC dependent of the load.

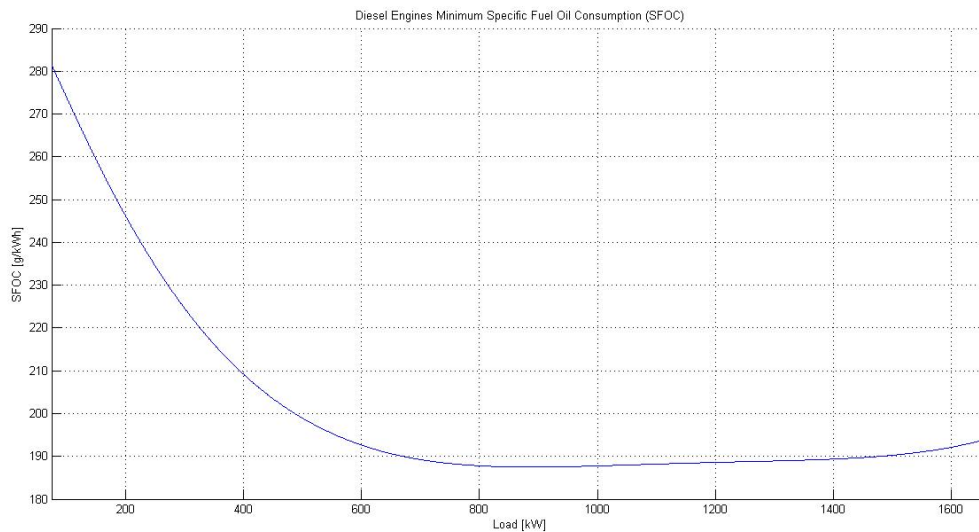


Figure 29

6.2 Synchronous generator

6.2.1 Ratings and specifications

The recommended generator to use in combination with the Wärtsilä 9L20 diesel engine is a 1980 kVA synchronous generator. [3.1]

The ratings and specifications of the selected synchronous generator are listed in the table below.

S_N	1980 kVA
$U_{RMS,N}$	690 V
L_S	0.12 mH
Pole pairs	4
Rated speed	900 RPM
Frequency	60
I_F	25 A

Table 8

6.2.2 Investigation of the excitation system

The excitation curve for the generator is obtained from a standard in Simulink. It does not provide any accurate values, but still it gives a useful insight into which speed and field current that is required in different load situations.

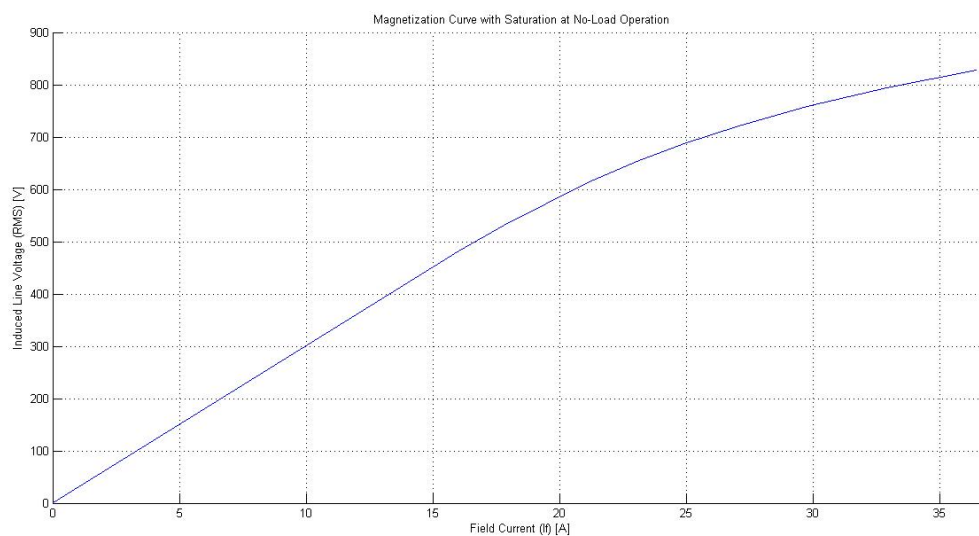


Figure 30 Excitation curve for no-load operation at rated speed [5.1]

The curve is obtained by using ten known plots of the excitation curve.

I_F	E_{LL}
0.0000	0.000
16.0100	483.000
17.8175	531.162
21.1025	612.168
23.0350	653.154
24.8900	687.861
27.0500	721.740
29.7500	759.000
32.9000	794.190
36.4250	828.690

Table 9 [5.1]

Equation 35 is solved with respect to K with the values from table 9 at rated speed.

$$K = \frac{E_{LL}}{I_F * n} [70]$$

The values for K is presented in table 10.

I_F	K
16.0100	0.0335
17.8175	0.0331
21.1025	0.0322
23.0350	0.0315
24.8900	0.0307
27.0500	0.0296
29.7500	0.0283
32.9000	0.0268
36.4250	0.0253

Table 10

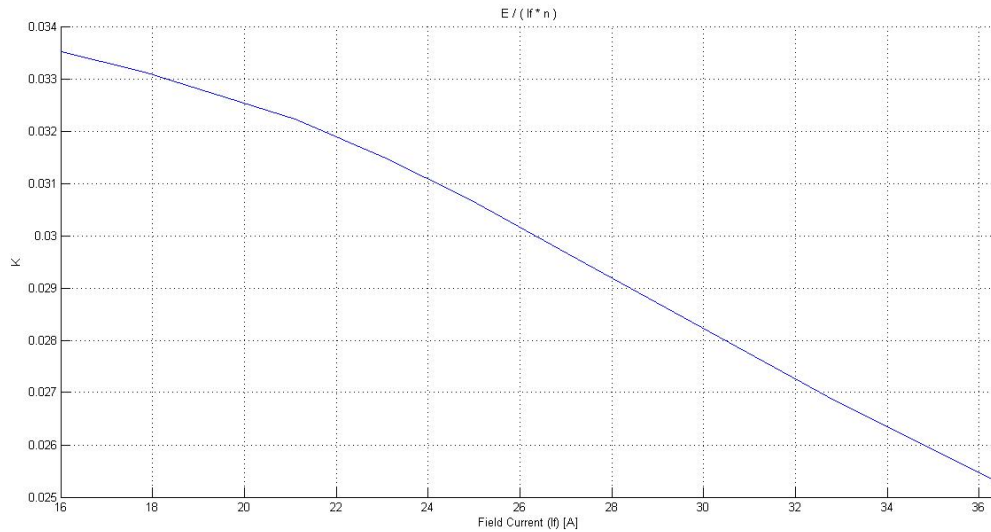


Figure 31 Characteristics of the K-values at rated operation, with increasing field current

The K-value decreases as the field current increases, due to the saturation of the rotor iron, as explained in chapter 4.3.

With the K-value known, the saturation curve for different speeds than the rated speed can be calculated. This makes it possible to determine the synchronous generator's load dependent minimum speed.

6.3 Diode based DC-distribution system

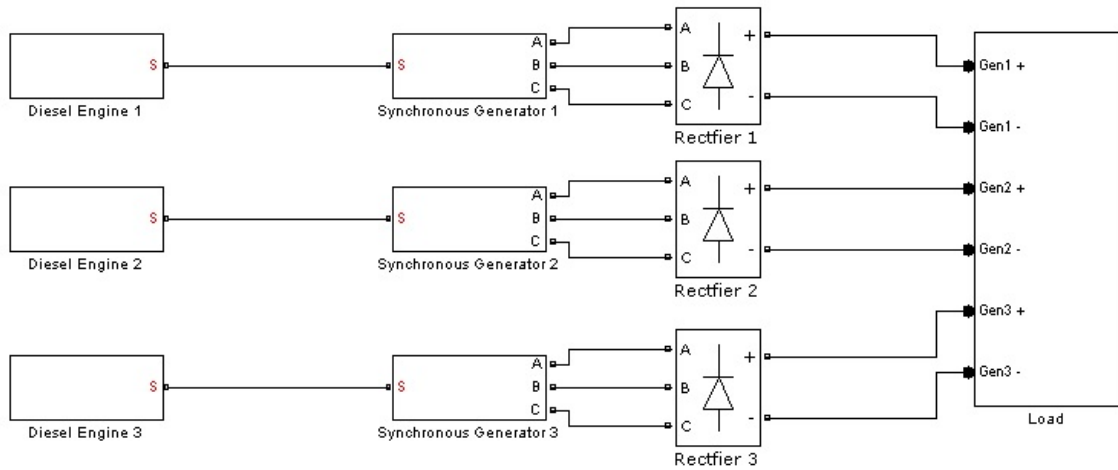


Figure 32 Diode based DC-distribution system

6.3.1 Minimum speed

To be able to calculate the fuel consumption the minimum speed at each load situation has to be obtained.

To determine the minimum speed the system needs to deliver the required power and voltage there are two factors that have to be taken into consideration. The diesel engine must be able to provide the power at the given speed and the synchronous generator must be able to generate the desired voltage at this speed.

The voltage at the DC-bus is set to be 931.5 volt, which is the DC-voltage the synchronous generator generates at no-load operation, with rated speed and excitation current.

The calculation has the nominal speed as starting point to determine an approximately minimum speed in the given load situation.

6.3.1.1 Procedure for calculating of the minimum speed of the diesel generator set

The no-load DC-voltage is calculated by solving the expression in equation 55 with respect to V_{d0} .

$$V_{d0} = V_d + \frac{3 * I_d * \omega_N * L_s}{\pi} \quad [71]$$

The ratio between V_d and V_{d0} is then calculated as presented in equation 72.

$$\frac{V_d}{V_{d0}} = \frac{V_d}{V_d + \frac{3 * I_d * \omega_N * L_s}{\pi}} = \frac{1}{1 + \frac{3 * I_d * \omega_N * L_s}{\pi * V_d}} \quad [72]$$

The ratio $\frac{V_d}{V_{d0}}$ is used in figure 22 to determine the ratio between I_d and the short circuit current I_{sc} .

The power factor is determined by applying the ratio $\frac{I_d}{I_{sc}}$ in figure 23.

The apparent power is calculated with the power factor found in figure 23.

$$S = \frac{P_{Load}}{PF} [73]$$

This is the power the diesel engine has to deliver.

The required line voltage from the generator is calculated from the value of V_{d0} obtained in equation 71.

$$V_{LL} = V_{d0} * \frac{\pi}{3 * \sqrt{2}} [74]$$

The angle of the line voltage is set to zero.

The line current is determined in equation 75.

$$I_L = \frac{P_{Load}}{\sqrt{3} * V_{LL} * PF} [75]$$

The angle of the line current is then calculated using the power factor found in figure 23.

$$\varphi = \cos^{-1}(PF) [76]$$

The synchronous reactance is calculated as shown in equation 77.

$$X_S = \omega_N * L_S [77]$$

The necessary induced voltage is calculated from the information obtained in equation 74, 75, 76 and 77. For simplicity, the armature resistance is neglected calculating the induced voltage.

$$E_{LL} = V_{LL} + \sqrt{3}(I_L \angle(-\varphi) * X_S \angle 90^\circ) [78]$$

The diesel engines minimum speed is calculated by solving equation 65 with respect to n , using the apparent power found in equation 73.

$$n_{mec_{min}} = \sqrt[3]{\frac{S}{k_{mec}}} [79]$$

The synchronous generator's minimum speed is derived by solving the formula in equation 35 with respect to n . The values for the highest excitation current is used for E_{LL} , K and I_F .

$$n_{el_{min}} = \frac{E_{LL}}{K_{I_{Fmax}} * I_{Fmax}} [80]$$

The minimum speed calculated will be higher than the actual minimum speed, as the synchronous reactance is calculated using the rated speed, and not the minimum speed.

The process is repeated with the calculated minimum speed replacing the rated speed in the calculations.

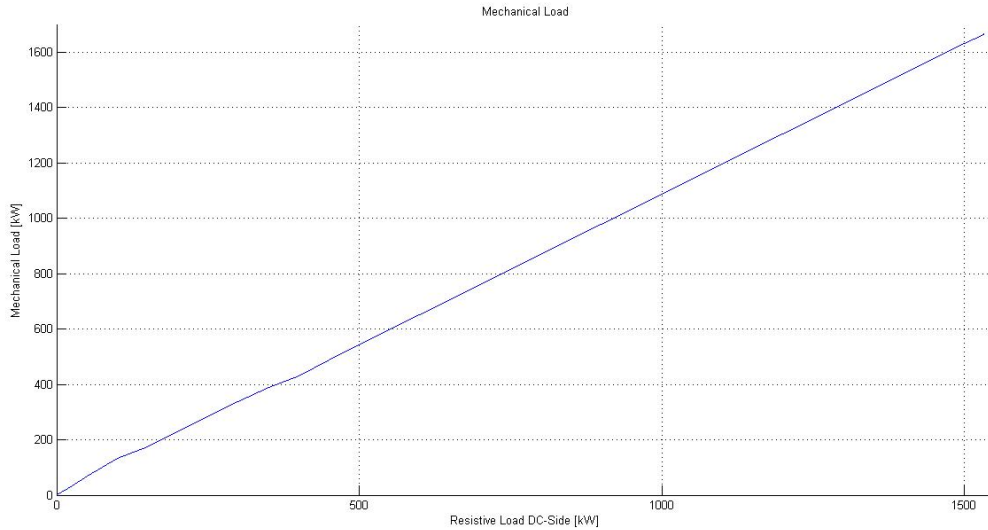


Figure 33 Load on diesel engine

The graph shows that the diesel engine reaches its maximum load level, 1665 kW, when the resistive load on the DC-side is 1531.8 kW.

This is neglected in the calculation of the fuel savings, as mentioned in chapter 6.

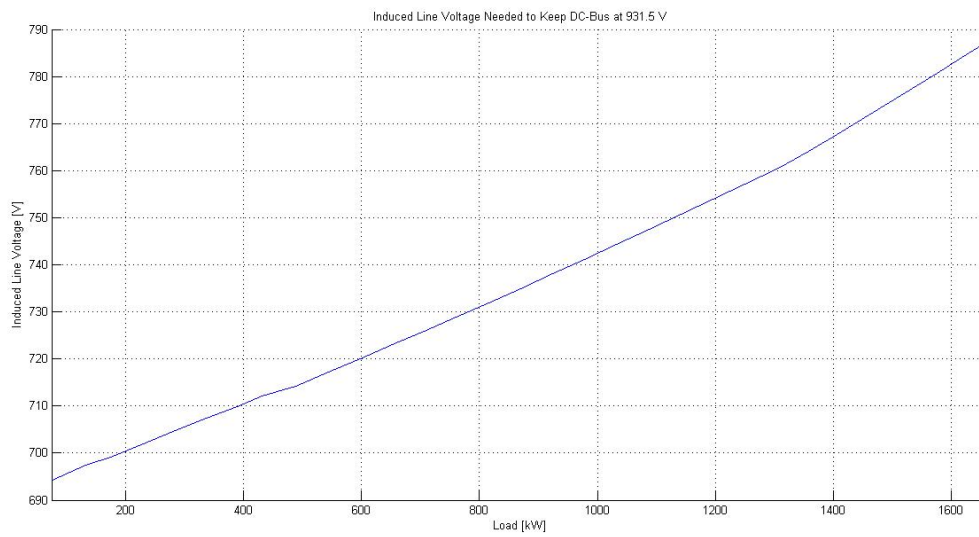


Figure 34 Necessary induced line voltage

The minimum speed dependent of the load is presented by the graph in figure 35.

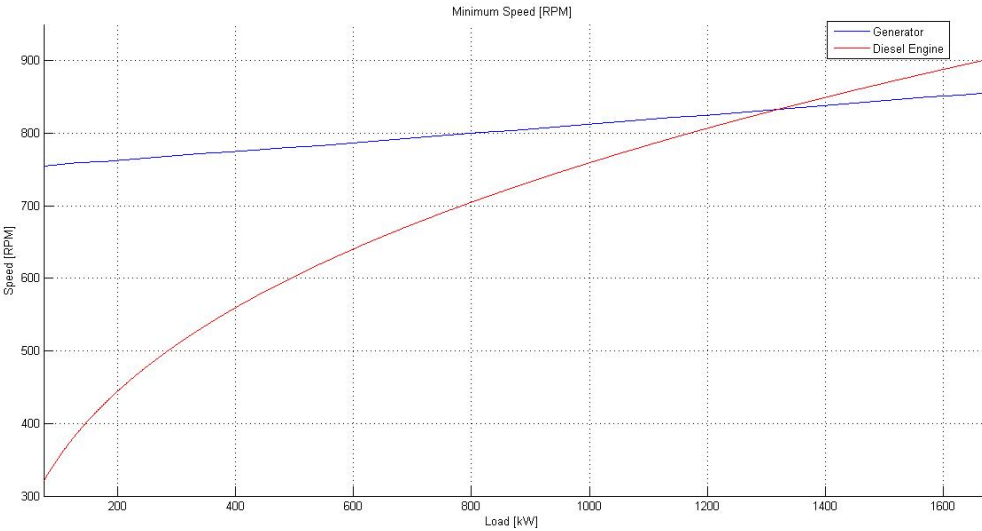


Figure 35 Minimum speeds of the synchronous generator and diesel engine

As illustrated by the graph in figure 35, the minimum speed of the supply system is limited by the generator up to 1321 kW. When the load exceeds 1321 kW the minimum speed is limited by the diesel engine.

The minimum speed of the system will follow the graph in figure 36.

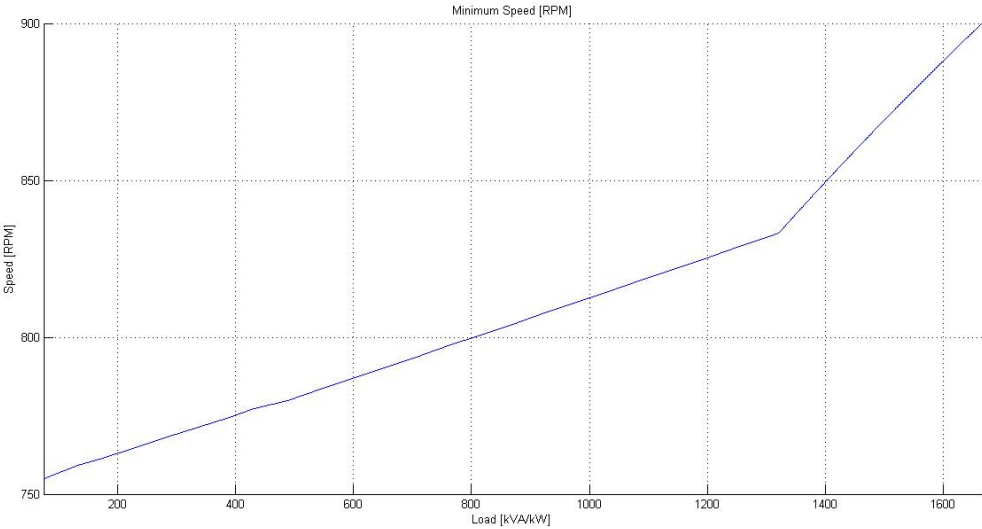


Figure 36 Minimum speed of the system

6.3.2 SFOC-characteristics

The SFOC-characteristics for the three alternative running operations for this supply system is presented in figure 37.

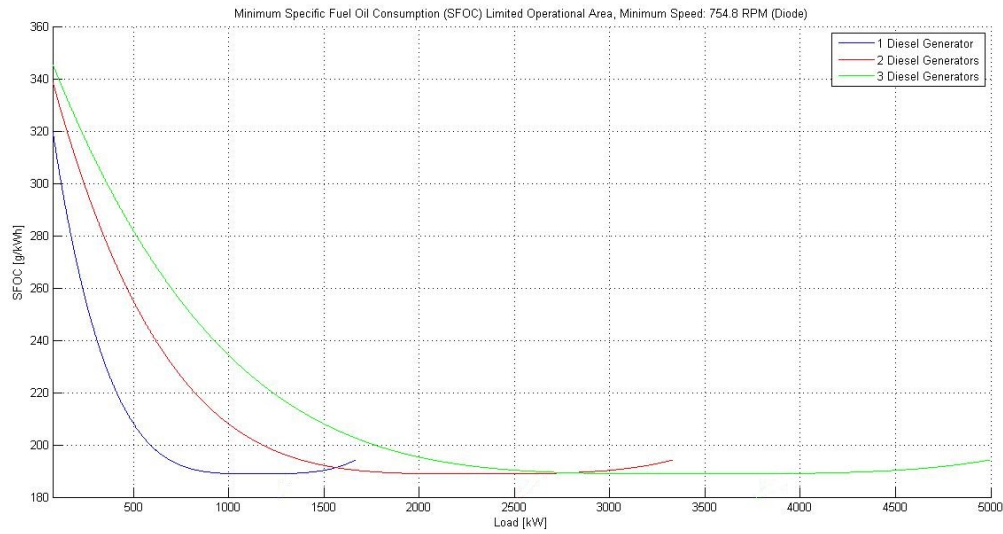


Figure 37 SFOC-characteristics

The intersection between the graphs indicates where it is optimal to change the number of running diesel generators to obtain the lowest SFOC. The intersection between the operation running one diesel generator, and the operation running two diesel generators, is occurring when the load is 1565 kW.

The intersection point between the operation of two diesel generators, and the operation of three diesel generators, is when the load is 2783 kW.

6.4 AFE based DC-distribution system

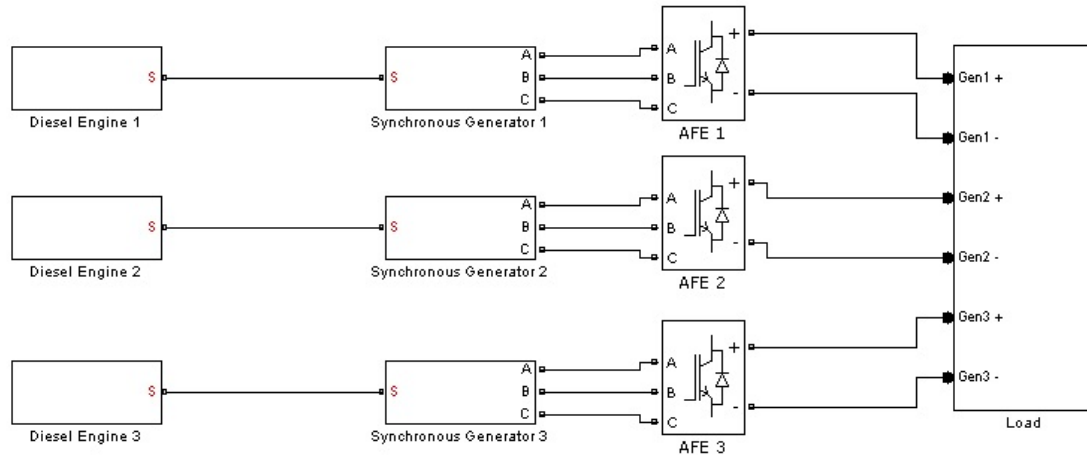


Figure 32 AFE based DC-distribution system

6.4.1 Minimum speed

The AFE rectifier is able to boost the DC-voltage to a value around ten times the peak value of the input voltage as mentioned in chapter 5.3. The calculation starts therefore with the assumption that the mechanical minimum speed is the systems minimum speed at all load situations.

The load dependent minimum speed of the diesel engine is presented in figure 39.

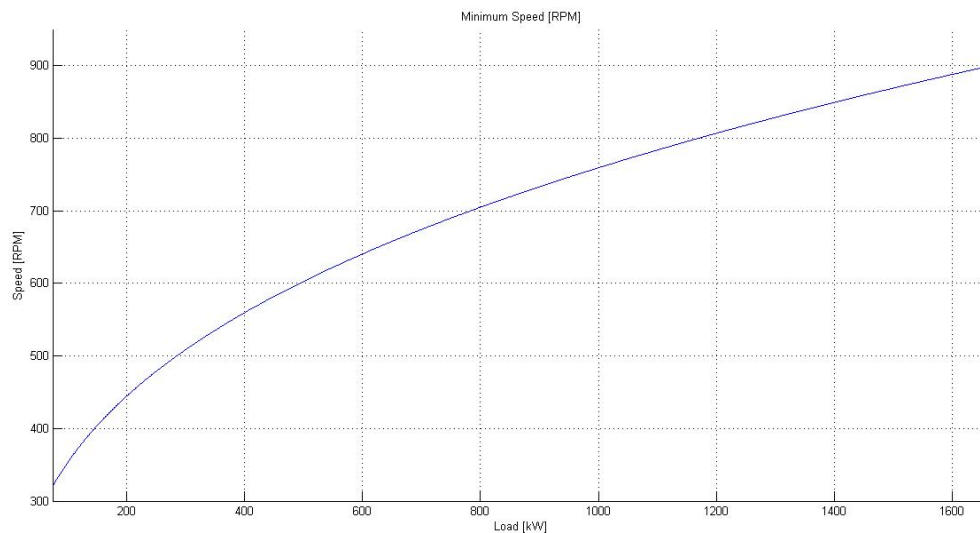


Figure 39 Minimum speed of the diesel engine

From equation 35 the induced voltage at the minimum mechanical speed is found.

$$E_{LL} = K_{I_{F_{max}}} * I_{F_{max}} * n_{mec_{min}} \quad [81]$$

The line current is calculated by using the load of the system and the known induced voltage E_{LL} .

$$I_L = \frac{P_{Load}}{\sqrt{3} * V_{LL} * PF} \quad [82]$$

The value found for I_L in equation 82 will be lower than the actual current, as the voltage drop over the synchronous reactance is neglected in the calculation.

The power factor for the AFE rectifier is assumed to be approximately one. The angle of the current is therefore considered to be zero.

The synchronous reactance at this speed is found by inserting the minimum speed of the diesel generator in equation 83.

$$X_s = \omega_{mec_{min}} * L_s \quad [83]$$

The armature resistance is neglected.

The line voltage is calculated in equation 84.

$$V_{LL} = E_{LL} \angle \varphi - \sqrt{3} (I_L \angle 0^\circ * X_s \angle 90^\circ) \quad [84]$$

The angle of the line voltage is set to zero. As the angle of the line current also is assumed to be zero and the armature resistance is neglected, the angle of the induced voltage can be calculated as shown in equation 85.

$$\varphi = \cos^{-1} \frac{\sqrt{E_{LL}^2 - (I_L * X_s)^2}}{E_{LL}} \quad [85]$$



Figure 40 Line voltage at diesel engines minimum speed

The induced voltage at the diesel engines minimum speed is within the range of the AFEs boost ability. The supply system can therefore utilize the entire operational area of the diesel engine.

6.4.2 SFOC-characteristics

The SFOC-characteristics for the three alternative running operations for this supply system is presented in figure 41.

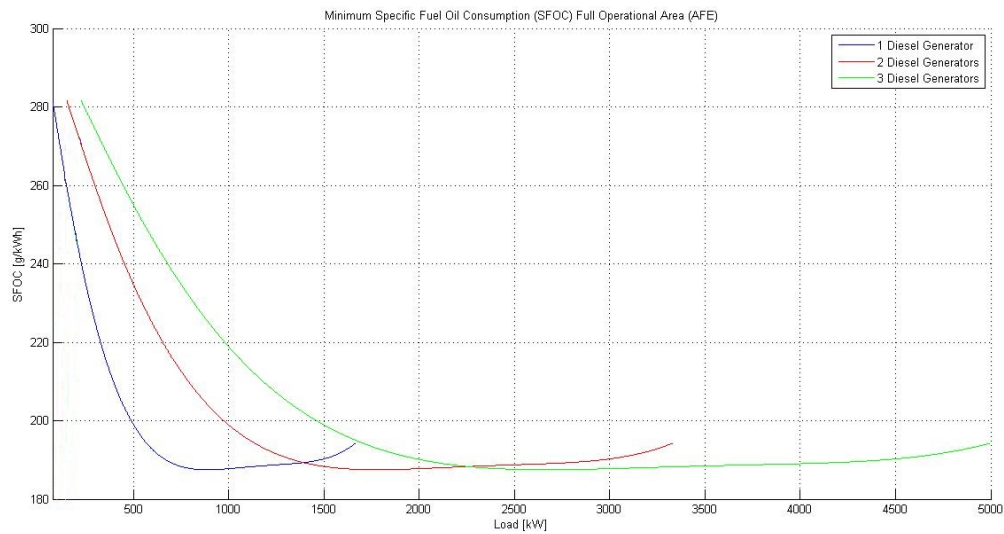


Figure 41 SFOC-characteristics

The intersection between the operation running one diesel generator and the operation running two diesel generators occurs when the load is 1394 kW.

The intersection point between the operation of two diesel generators and operation of three diesel generators occurs when the load is 2255 kW.

6.5 AC-based distribution system

6.5.1 Minimum speed

The speed of the system is fixed to 900 RPM for all load situations.

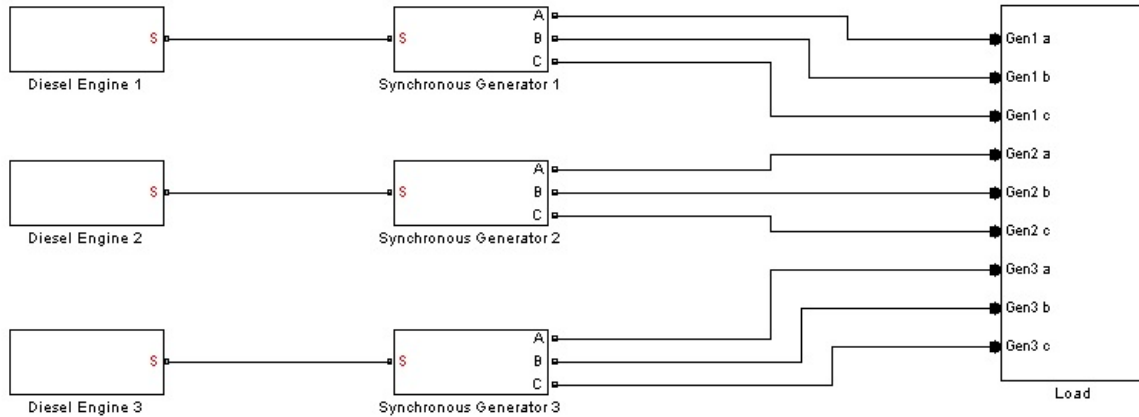


Figure 42 AC-based distribution system

6.5.2 SFOC-characteristics

The SFOC-characteristics for the three alternative running operations for this supply system are presented in figure 43.

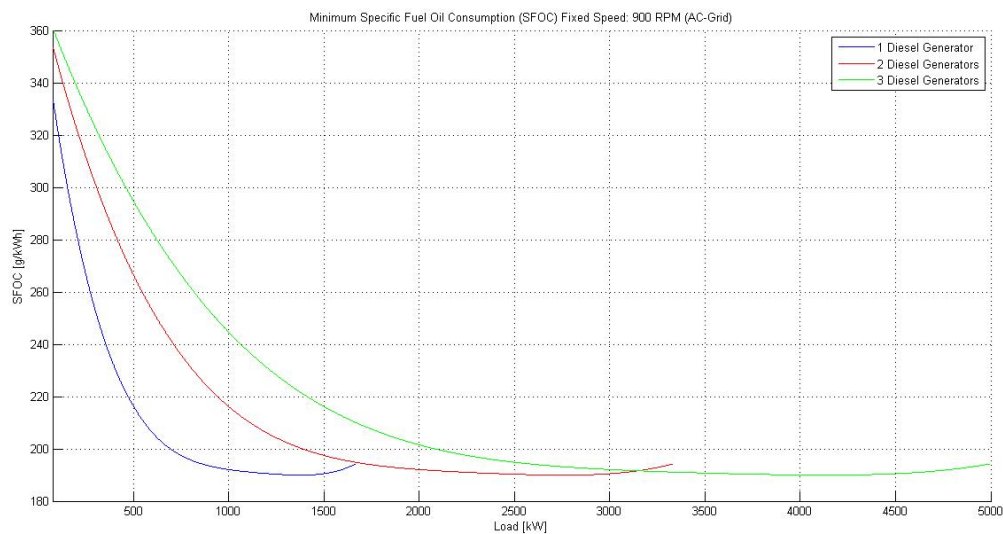


Figure 43 SFOC-characteristics

The SFOC-curve of the operation running one diesel generator will not intersect with the SFOC-curve of the operation running two diesel generators in this supply solution. The SFOC of the operation running two diesel generators will not achieve a SFOC as low as the operation running one diesel generator before the maximum loading of one diesel generator is reached at 1665 kW. There will therefore be a small drop in the system's efficiency from the 1665 kW load to the 1666 kW load.

The intersection point between the operation of two diesel generators and operation of three diesel generators is when the load is 3149 kW.

6.6 Comparison of the distribution systems

6.6.1 Diode based DC-distribution system compared to an AC-based distribution system

In figure 44 the two distribution systems' SFOC-characteristics are presented.

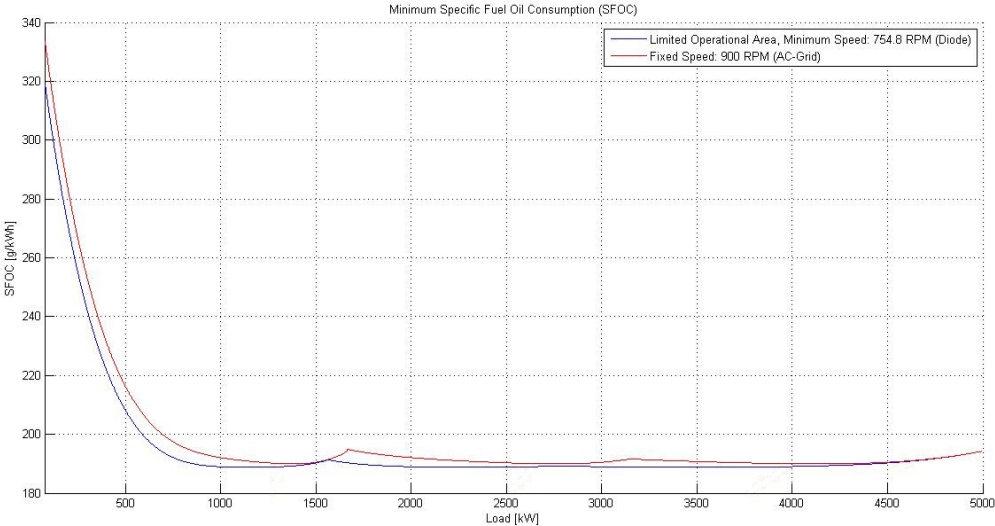


Figure 44

In figure 45 the difference in SFOC between the two distribution systems is presented.

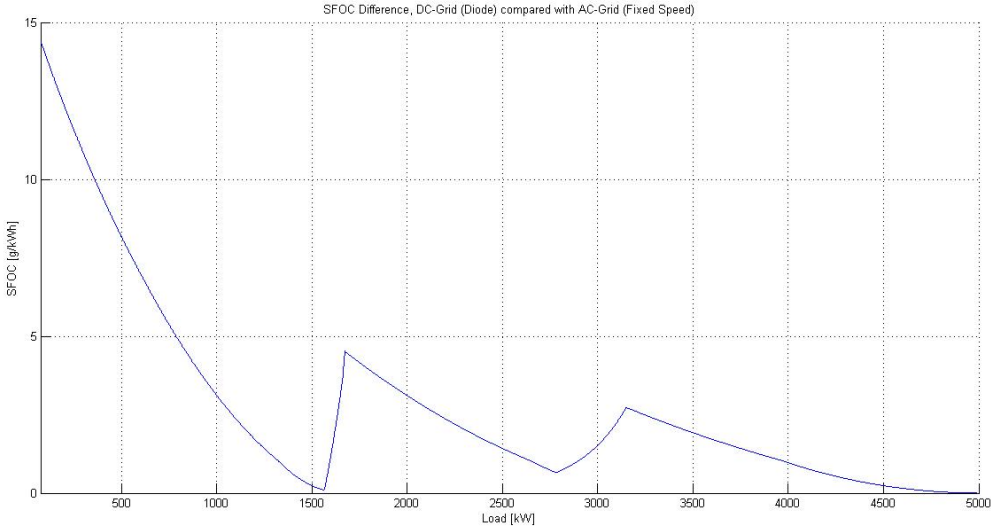


Figure 45

The fuel savings are obtained with the procedure presented below:

$$\Delta SFOC \left(\frac{g}{kWh} \right) = SFOC_{System_1} - SFOC_{System_2} \quad [86]$$

$$\Delta FOC \left(\frac{g}{h} \right) = \Delta SFOC * Load \quad [87]$$

$$\text{Density of petroleum diesel} = 832 \left(\frac{g}{l} \right) \quad [88]$$

$$\text{Fuel savings} \left(\frac{l}{h} \right) = \frac{\Delta FOC \left(\frac{g}{h} \right)}{\text{Density of petroleum diesel} \left(\frac{g}{l} \right)} \quad [89]$$

The fuel savings and percentage fuel savings are illustrated in figure 46 and 47.

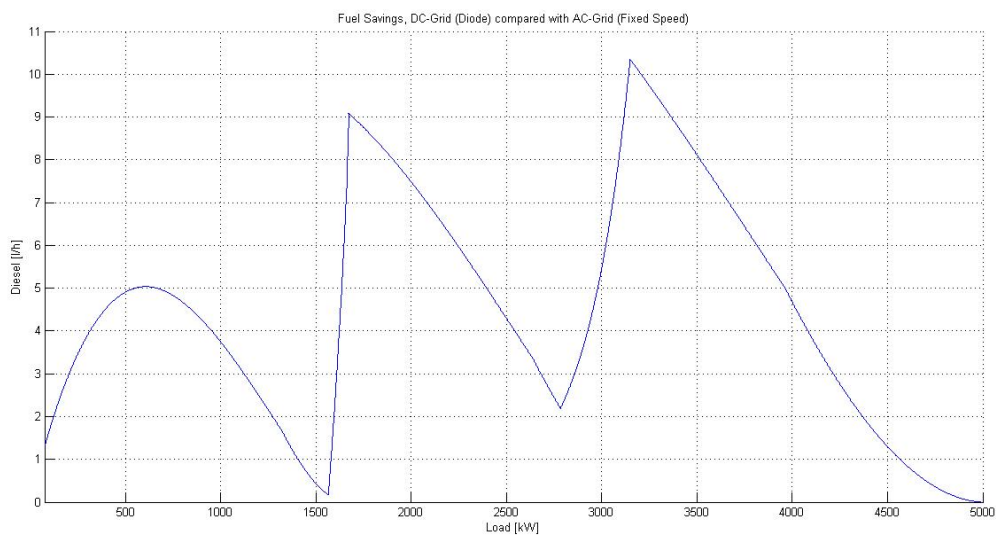


Figure 46

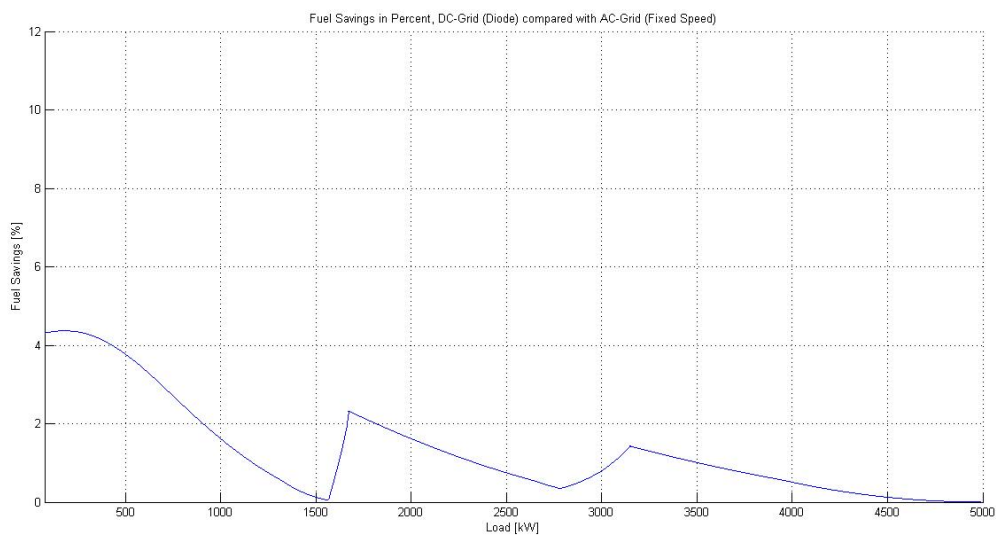


Figure 47

At low loads there is a large rotational speed difference between the two supply systems, which causes the SFOC difference to be very high. The first peak value of the fuel savings occurs at 611 kW. At this load the fixed speed configuration runs at 900 RPM while the solution with diode rectifiers is running at 787.6 RPM. This causes the pressure in the diesel engines cylinders to be higher, consequently increasing the efficiency.

The diode based solution is able to run two diesel generators with low SFOC from 1565 kW. The difference in fuel consumption will increase until the load exceeds 1665 kW and the fixed speed solution can run two diesel generators at satisfying efficiency. The fuel savings second peak value will therefore occur when the loading exceeds 1665 kW.

The third peak value occurs at 3149 kW. The diode based solution is able to run three diesel generators from 2783 kW, and the difference will increase up to 3149 when the fixed speed solution is switching from running two diesel generators to three diesel generators.

6.6.2 Diode based DC-distribution compared with AFE based DC-distribution

The SFOC characteristic of a DC-grid where the power is supplied by diode rectifiers is compared with a system which is supplied by AFE-rectifiers. The AFE based supply system can deliver the desired voltage in the entire operation area of the diesel engine.

The SFOC characteristics of the two supply systems is presented in figure 48.

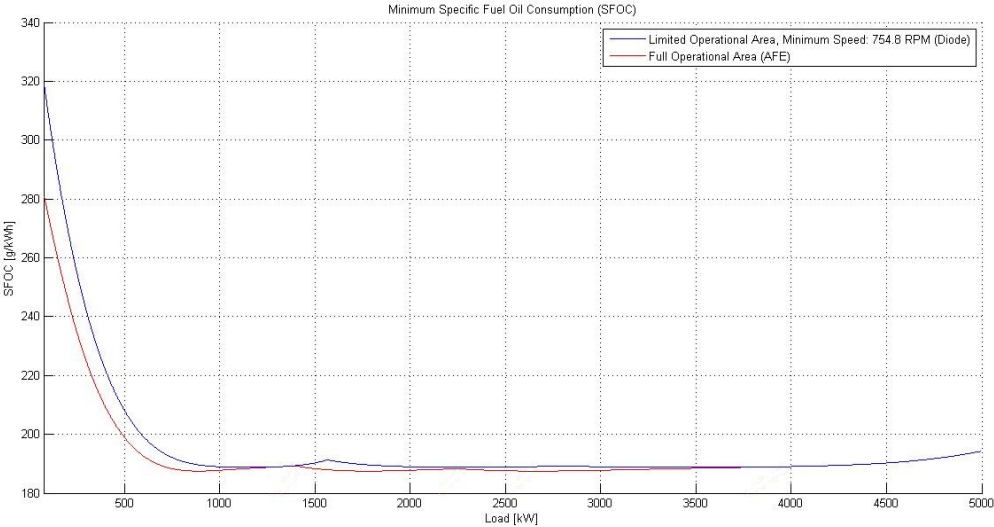


Figure 48

In figure 49 the difference in SFOC between the two configurations is presented.

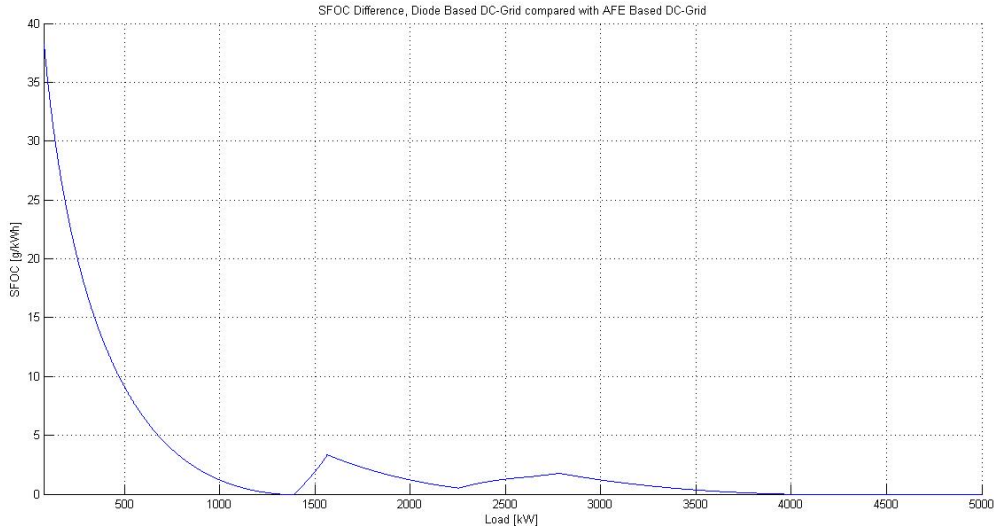


Figure 49

The fuel savings and percentage fuel savings are presented in figure 50 and 51. The procedure for calculating the fuel savings is the same as in the previous chapter.

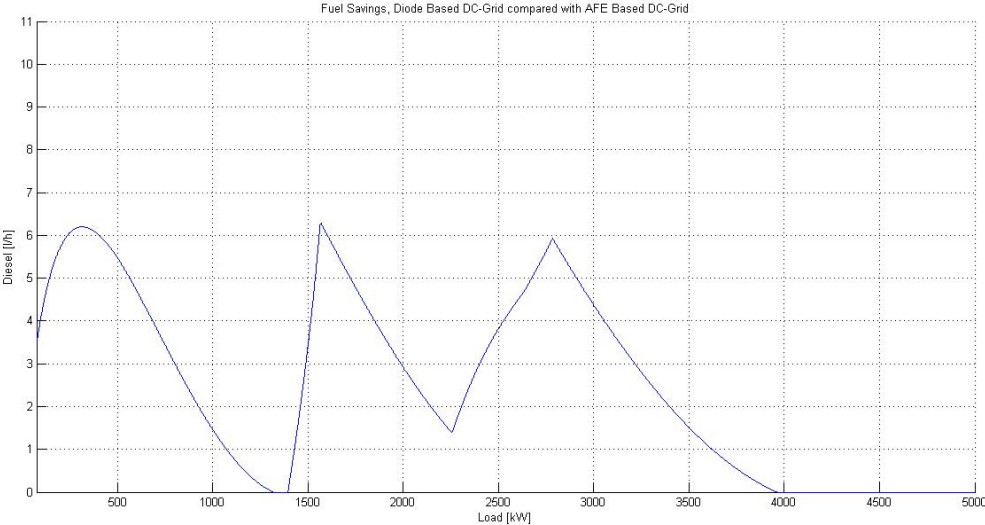


Figure 10

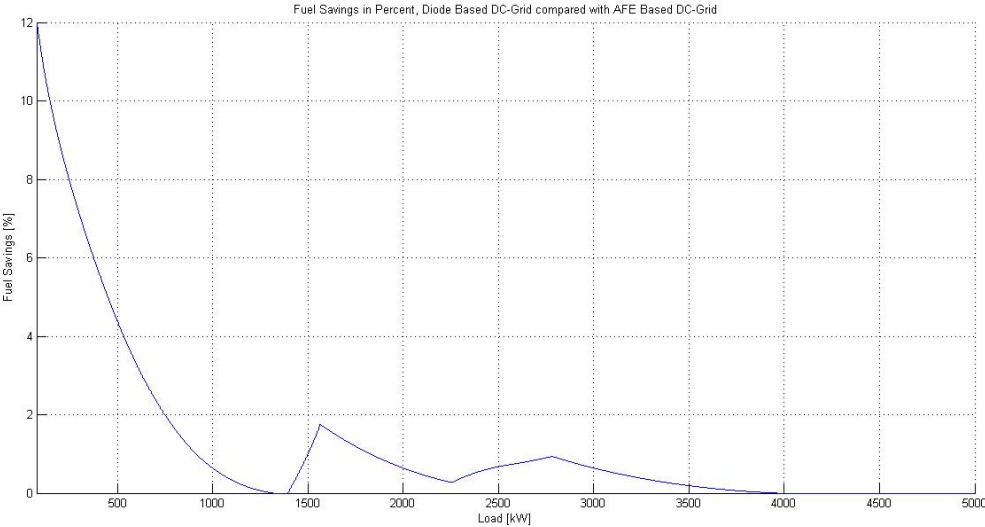


Figure 51

The first peak of the fuel savings appears at 315 kW. At this load it is possible for the system with AFE rectifiers to run at a speed as low as 516.7 RPM, while the diode based system has to run at 770.1 RPM to obtain the voltage level on the DC-bus. Due to the large speed difference, there will also be a large difference in the fuel consumption between the two supply systems.

The second peak value occurs at 1564 kW. The AFE based system is able to run two diesel generators at high efficiency from 1394 kW. The difference between the two systems' is that the fuel consumption will increase until the diode based system is able to switch from running one diesel generator to two diesel generators, which, as mentioned earlier, is at 1564 kW.

The second peak value occurs at 2783 kW. The AFE based solution is able to operate with three diesel generators from 2255 kW. The difference in fuel consumption will increase from this load until the

load reaches 2783 kW, when the diode solution switches from running two diesel generators to three diesel generators.

The solution utilizing AFE rectifiers are able to operate at much lower speeds at low loads than the solution with diode rectifiers. At low loads the efficiency of the AFE based system is therefore far better than the efficiency of the diode based system

At higher loads the mechanical minimum speed will be higher than the minimum speed of the generators in the diode based system. The diode based system will then be able to operate at the same speed at the AFE based system, and the SFOC of the two systems will be equal.

7. Discussion and conclusion

7.1 The diode based DC-distribution system compared to the traditional AC-distribution

From the calculations made in this thesis the introduction of a diode based DC-grid as replacement for the traditional AC-distribution on board ships, represents relative high percentage fuel savings at low loads. The maximum percentage fuel savings is 4.37 % and occurs at 177 kW. At low loads the difference between the diode based DC-distributions speed and the AC-grids fixed speed is at its maximum level.

At higher loads, the difference between the two distribution systems' speed is lower, and consequently the percentage fuel savings is reduced.

The diode based DC-distribution system is able to divide the load at several diesel generators with high efficiency at lower loads than the AC-distribution system. This causes the percentage fuel savings to increase from the load situation where the diode based DC-grid is able to switch in one more diesel generator, until it peaks when the AC-distribution system is able to switch in the extra diesel generator.

The largest percentage fuel savings is, as previously mentioned, at low loads, but as the total fuel consumption also is relative low at these load situations, the actual fuel savings is small.

The maximum fuel savings in liter per hour is achieved at the load situations where the diode based DC-distribution system is able to divide the load at more diesel engines than the AC-distribution system, as explained in the previous paragraph. The maximum fuel savings is 10.35 liter per hour, and it occurs at 3149 kW, right before the AC-distribution system is able to switch from running two diesel generators to running three diesel generators.

7.2 The diode based DC-distribution system compared to the AFE based DC-distribution system

The DC-distribution system utilizing active front-end rectifiers is able to run at the diesel engines minimum speed in all load situations. The minimum speed of the diode based DC-distribution system is 754.8 RPM, while the AFE based DC-distribution system has a minimum speed of 320.23 RPM. This large difference in the two supply systems' minimum operating speed causes the percentage fuel saving at low loads to be very high. At this thesis minimum load level 75 kW, the percentage fuel savings by replacing the diode based DC-distribution system with an AFE based DC-distribution system, will be as high as 12 percent. Due to the low fuel consumption at this load, the actual fuel savings will not be higher than 3.5 liter per hour.

The highest actual fuel savings while both systems runs one diesel generator set is at 315 kW. The total fuel consumption will be relatively low in this load situation, but as the speed difference is high, almost 254 RPM, the efficiency of the AFE based DC-distribution system will be far better than the efficiency of the diode based DC-distribution system. The actual fuel savings in this load situation will be as large as 6.2 liter per hour, a percentage fuel saving around 6.9 %.

The AFE based DC-distribution system is able to utilize two diesel generator sets from 1394 kW. The maximum actual fuel saving occurs when the load reaches 1565 kW, before the diode based DC-distribution system is able to couple in a second diesel generator set. The fuel savings at this load situation will be 6.3 liter per hour.

The fuel savings by introducing a diode based DC-distribution system is relatively high. Whether the fuel savings is able to defend the cost of installing the system is not being investigated in the thesis.

The simplification, where the loss in the rectifiers and the poor power factors effect on the power drawn from the diesel engine is neglected, causes the calculated fuel savings to be larger than the actual fuel savings. This has to be considered when calculating the cost.

The issue regarding poor power factor is avoided when the diode rectifiers is replaced by AFE rectifiers. The power loss in the AFE rectifier is higher than the losses in the diode rectifier. This is neglected in the calculation of the fuel savings. The consequence of this simplification is not as severe as they could have been, as they to some degree are added up by the simplifications in the calculation of the fuel consumption in the diode based DC-distribution system.

The cost of installing an AFE based DC-distribution system on board ships is very high compared to the diode based DC-distribution system.

A factor that is not considered in the thesis is that the AFE based DC-distribution system not necessarily has to be supplied by a synchronous generator. Due to the AFEs ability to control the voltage and the reactive power component in the system, it is possible utilize induction generators for the power supply on board the ship.

Induction generators represent many advantages, such as; simple construction, low maintenance requirements, simple control, low cost and general robustness. The introduction of induction generators will therefore decrease the total cost of installing an AFE based DC-distribution system on board ships.

7.3 Conclusion

The conclusion drawn from the investigations in this thesis is that vessels which experience frequent low load situations will benefit from introducing an AFE based DC-distribution system on board.

Vessels, which for the most part experience high load situations, the extra cost of investing in AFE-rectifiers cannot be justified, as the fuel savings will be virtually zero at high loads. For these vessels it will be expedient to replace the AC-distribution with the less expensive diode based DC-distribution system.

9. References

9.1 Literature

[1.1]

Hansheinrich Meier-Peter, Frank Bernhardt, "Compendium Marine Engineering, Operation - Monitoring - Maintenance", First edition.

[1.2]

Richard van Basshuysen, Fred Schäfer, "Internal Combustion Engine Handbook - Basics, Components, Systems, and Perspectives".

[1.3]

Svein Bua, Magnus Dalva, Olav Vaag Thorsen, "Roterende elektriske maskiner", Second edition.

[1.4]

Stephen J. Chapman, "Electric Machinery Fundamentals", Third edition.

[1.5]

Ned Mohan, Tore M. Undeland, William P. Robbins, "Power Electronics, Converters, Applications and Design", Third edition.

[1.6]

Jai P. Agrawal, "Power Electronic Systems, Theory and Design".

[1.7]

Chung-Chuan Hou, Po-Tai Cheng, Subhashish Bhattacharya, Jarsun Lin, "Modeling and Control of Three-Phase Active front-end Converters", IEEE, 2007.

9.2 Web-based literature

[2.1]

<http://cleantech.cnss.no/wp-content/uploads/2011/05/1998-Norwegian-Society-of-Chartered-Engineers-95-years-of-diesel-electric-propulsion-form-a-mekeshift-solution-to-a-modern-propulsion-system.pdf>

[2.2]

[http://www05.abb.com/global/scot/scot271.nsf/veritydisplay/441ce50a20b6169bc1257a25002efdc/\\$file/28-33%20m212_EN_72dpi.pdf](http://www05.abb.com/global/scot/scot271.nsf/veritydisplay/441ce50a20b6169bc1257a25002efdc/$file/28-33%20m212_EN_72dpi.pdf)

[2.3]

<http://faculty.ksu.edu.sa/eltamaly/Documents/Courses/EE%20339/Alternator.pdf>

[2.4]

<http://mediatoget.blogspot.no/2011/04/armature-reaction-armature-reaction-is.html>

[2.5]

<http://www.ee.lamar.edu/gleb/power/Lecture%2007%20-%20Synchronous%20machines.pdf>

[2.6]

http://1stmuse.com/atlas/permeability_and_magnetic_saturation/

[2.7]

[http://www04.abb.com/global/seitp/seitp202.nsf/c71c66c1f02e6575c125711f004660e6/a733e317b00f7c65832574f000513fd8/\\$FILE/A+team+of+drives.pdf](http://www04.abb.com/global/seitp/seitp202.nsf/c71c66c1f02e6575c125711f004660e6/a733e317b00f7c65832574f000513fd8/$FILE/A+team+of+drives.pdf)

[2.8]

http://www.isep.pw.edu.pl/icg/pdf/phd/mariusz_cichowlas.pdf

9.3 Literature regarding the diesel engines specifications and efficiency calculation

[3.1]

Product Guide Wärtsilä 20 - 3/2009.

[3.2]

SFOC/FOC calculation model delivered by SINTEF.

9.4 E-mail correspondence

[4.1]

E-mail correspondence with Lars Tandle Kyllingstad at SINTEF.

9.5 Information obtained from standards in Simulink

[5.1]

Saturation curve obtained from an example in Simulink.